Dynamic Stall Investigations on NACA0012 and OA209 Airfoils

By
C. Barla*, W. Geissler+, E. Berton*, M. Raffel+, D. Favier*

* Laboratoire d'Aérodynamique et de Biomécanique du Mouvement
CNRS & Université de la Méditerranée
163 Av de Luminy, Case 918, 13288 MARSEILLE Cedex09, France
Tel: 33 491 266030; Fax: 33 491 411691
eric@morille.univ-mrs.fr
+ DLR – Institute of Aerodynamics and Flow Technology,
Bunsenstrasse 10, Goettingen, D37073 Germany
Tel: +49 551 709 2353; Fax: +49 551 709 2811

Abstract

This paper presents a collaborative study between DLR and LABM on dynamic stall process. The present investigation deals with both numerical as well as experimental tools on conventional NACA0012 and OA209 typical 3D helicopter airfoils. The main goal of this investigation is to better understand the different flow phases during light and deep dynamic stall process. Indeed, the effects of the boundary layer transition from a laminar state to a turbulent one play an important role with respect to the unsteady flow development. A recently developed transition model, implemented in the DLR numerical code, has been used and the calculated results have been compared with corresponding experimental data. A new transition onset criterion, developed at LABM, has also been implemented in the numerical and some results have been obtained with this model.

Notations

a	Speed of sound, (m/s)
c	Airfoil chord, (m)
f	Oscillations frequency, (Hz)
k	Reduced frequency of oscillation, ($k=c.\omega/2.U_\infty=\pi.f.c/U_\infty$)
M	Mach number: (U_∞/a)
Re	Reynolds number, ($U_\infty.c/\nu$)
U_e	Mean local external velocity, (m/s)
U_∞	Freestream velocity, (m/s)
x, y, z	Tangential normal and spanwise coordinate at the airfoil surface, (m)
α	Angle of attack of the airfoil, (deg)
δ_2	Momentum loss thickness, (m) $\delta_2 = \int_0^\delta \frac{u}{U_e}(1-\frac{u}{U_e})dz$
δ'_3	Second thickness of energy of the boundary layer, (m), $\delta_3' = \int_0^\delta \frac{u^2}{U_e^2} * (1-\frac{u}{U_e})dz$
ω	Rotational frequency, ($rad.s^{-1}$)
Ω	Non dimensional local vorticity

Introduction

For the problem of dynamic stall it has been found by numerical as well as experimental investigations (Ref. 1 and 2) that free transition of the flow from laminar to turbulent may play a dominant role with respect to unsteady flow characteristics. In particular at low Reynolds numbers ($<10^5$) transition develops over a major part of the airfoil upper surface during the oscillatory motion. The effects of transition on dynamic stall characteristics are then no longer negligible.

Recently, the present Navier-Stokes code (Ref. 3) has been equipped with a transition model which is based on the Chen-Tyson exponentially growth model (Ref. 4) combined with Michel's criterion for the determination of transition onset based on the momentum loss thickness δ_2 (Ref. 5). The latter method has been compared with experimental data and has shown its potential to improve the results (Ref. 6).

Several additional transition-onset models have been described and tested for the static and oscillating NACA0012 airfoil at $Re=10^5$ (Ref. 7). It was found that the onset criterion based on the energy loss thickness of second kind, δ'_3, gives improved results. The present

transition model has therefore been extended to also include the δ'_3-methodology. Some testing and calculations under both steady and dynamic stall conditions have been carried out with the new transition onset device.

At LABM a lot of expertise exists in the application of LDV-systems in combination with moving airfoil models (Ref. 8 and 9). The corresponding LDV test set up is called "Embedded LDV" (ELDV) which does express the fact that the LDV and its equipment are installed in the moving system. With this arrangement it is possible to measure details in the unsteady boundary layers at always the same position with respect to the moving model surface. The information, i.e. the flow velocities in tangential as well as in normal surface directions are available and can directly be compared with corresponding numerical data.

In the present study the 3D-version of the ELDV (Ref. 10) has been applied allowing also measuring the spanwise velocity component in addition. The present study has been done with rather small flow velocities (U_∞=5m/s) and Re-numbers at or below 10^5. The numerical code applied for this investigation is developed for compressible flow investigations and has been used for the first time for flow cases of M<0.1. In this flow regime the experimental frequency between 1Hz and 2Hz still leads to rather large reduced frequencies k>0.15. With this value rather strong hysteresis effects are to be expected during the dynamic stall process. It is further expected that laminar/turbulent separation bubbles will develop with transition taking place in the vicinity of these bubbles. Both numerical as well as experimental efforts will concentrate on the boundary layer velocity profile development. It is of special concern in the LDV measurements that reliable results are also obtained inside the bubble where only small amounts of tracer particles are available.

In addition to investigations of the NACA0012 airfoil the OA209 airfoil section as a typical helicopter rotor airfoil used on flying helicopters has been investigated as well.

This 9% thick airfoil has recently been chosen as a standard airfoil in the DLR/ONERA common project on dynamic stall. The OA209 will therefore be investigated under quite different flow conditions and the present study will add some important information concerning the low speed regime with emphasis placed on transition investigations.

Numerical tools

The numerical studies have been carried out with 2D unsteady Navier-Stokes code (Ref. 3) which uses the Approximate Factorization Implicit methodology originally developed by Beam and Warming (Ref. 11). The calculations are executed in a space fixed frame of reference, i.e. the curvilinear coordinates are fixed to the moving body as well as to the static outer frame. This arrangement needs the determination of a new grid for every time-step. These intermediate grids are obtained from the two grids in the extreme (minimum and maximum) incidence conditions by simple linear interpolation. The grids are of C-grid topology. The reason for choosing this procedure is the application of the present tools also for unsteady body deformations, i.e. for airfoils with leading or trailing edge flap motions, etc., (Ref. 1). The code has a steady component which allows the calculation of steady flow data as obtained after a sufficient number of time-steps. The steady version of the code is also working in the time-accurate mode.

For the modelling of transition in a numerical code based on the full equations, i.e. the Navier-Stokes equations it is first of all necessary to determine the correct edge of the boundary layer. This is achieved by calculating the product of distance from the surface and the local vorticity:

$$F = y_n / c \cdot \Omega \qquad (1)$$

with y_n as normal distance from the surface referred to the airfoil chord c and Ω as the local non dimensional vorticity. Marching outwards from the maximum of this function, F_{max}, the boundary layer edge δ is defined at the position, where the function F has been decayed to 50% of F_{max}. The determination of the momentum loss thickness δ_2 and the energy loss thickness δ'_3 can then be calculated from the definitions. From Michel (Ref. 5), a rather simple formula has been given to define the border between laminar flow and the onset of transition:

$$(\mathrm{Re}_{\delta_2})_{\mathrm{trans}} = 1.174 \cdot (1 + 22400/\mathrm{Re}_s) \cdot \mathrm{Re}_s^{0.46} \qquad (2)$$

Where the Reynolds number Re_s in (2) is based on the length s of the boundary layer from the stagnation point along the curved airfoil surface to the position under consideration:

$$\mathrm{Re}_s = \frac{U_\infty \cdot s}{\nu} \qquad (3)$$

A corresponding expression has been developed, (Ref.7), for the Reynolds number based on the energy loss thickness:

$$(\mathrm{Re}_{\delta_3'})_{trans} = 0.0135 \cdot (1+1.5 \cdot e^{-\frac{\mathrm{Re}_s}{35000}}) \cdot \mathrm{Re}_s^{0.8} \quad (4)$$

with $\mathrm{Re}_{\delta_2} = \frac{U_\infty \cdot \delta_2}{\nu}$ and $\mathrm{Re}_{\delta_{3'}} = \frac{U_\infty \cdot \delta'_3}{\nu}$ (5)

defining the Reynolds numbers based on momentum loss thickness and energy loss thickness respectively.

In the numerical calculations the procedure to determine transition onset either based on δ_2 or δ'_3 is now as follows:

It is assumed that the transition calculation can be done quasi-steady, i.e. for each single time-step separately. After the procedure to determine the outer edge of the boundary layer (1) has been finished, the velocity U_e and the boundary layer thickness δ are available at each chordwise station. The Reynolds numbers defined in (3) are then calculated next and compared with their defined values at transition onset (2) and (4). Transition onset is derived if the calculated Re-number distributions are crossing the defined functions, either (2) or (4).

In the experimental cases an indirect method has been applied, (Ref. 7), to find out if the measured velocity profile is located in the laminar or turbulent flow regime. For laminar type boundary layers, Pohlhausen's profiles are determined and the pressure gradient parameter is changed until a best fit with the measured profile is achieved. In cases of turbulent flows the thin boundary layer is approximated using the e^n-method and varying the n-exponent until a best fit is reached. This type of procedure however can only be applied for non-separated flows. For dynamic stall cases where severe flow separation occurs the procedure is not appropriate.

Different turbulence models have been implemented in the numerical code and have been tested for their applicability in different flow cases. For dynamic stall flow cases it has been shown that the Spalart-Allmaras (SA) one equation model, (Ref. 12), gives the most reliable results compared to experimental data. In addition the k-ω-SST model, (Ref.13), is also available. This two-equation model shows good results during the upstroke motion prior to severe separation however once separation occurs the model shows unrealistic high hysteresis effects including strong oscillations in the force and moment hysteresis loops.

In the present investigation the SA model has been used throughout.

Experimental Tools

1) ELDV Method

For each chord wise section selected, the flow survey is performed along the local normal to the model-surface (the altitude y_n ranging from about 0.1 mm to 100mm).

2D-velocimetry.

The Embedded Laser Doppler Velocimeter (ELDV) used for this survey in 2D flow has an optical head mounted on a supporting turntable linked to the oscillating frame as sketched in Fig.1. Moreover, it is equipped with a beam-expander to increase the focal distance to 400mm. This optical head is installed on an automated 2D-displacement device mounted itself on the turntable. The laser beams are so focusing from a 45° mirror in the boundary layer at the span wise locations considered. The supporting turntable is linked with the oscillating frame, so that U and V velocity components can be directly measured in the same reference frame as the oscillating boundary layer. A tele-driven system allows the adequate positioning of the measurement volume at any point of the airfoil surface (30cm in chord wise displacement). An angular sector provides the selection of the surveying normal direction, and the laser measurement volume can be displaced along the local normal to the surface with a displacement accuracy of 0.1mm. Due to the periodicity of the flow, each period is considered as a specific sample of the same phenomenon. So, each velocity component is recorded at each phase angle ωt ranging from 0° to 360° by steps of 1° over a large number of periods. Data are then statistically analyzed at prescribed values of the period, e.g. the instantaneous incidence, with an accuracy of : $\delta\alpha = 4\Delta\alpha/360 = 24/360 = 0.066°$. The acquisition time is stopped when 19,564 data have been stored, that generally requires about 150 periods.

3D-velocimetry.

The extension of the Embedded Laser Doppler Velocimetry (ELDV) method to the direct measurement of the 3D velocity field has been performed by means of special arrangements of mirrors and laser optical heads sketched at the top of Fig.1. The system consists of two optical heads mounted on a supporting turntable and attached to the oscillating frame (presented at the bottom of Fig.1).

2) PIV Investigations.

During the last two decades particle image velocimetry (PIV) has been considerably

improved for its application in wind tunnels. This technique allows the instantaneous measurement of the flow velocity in a large two-dimensional plane of the flow within a few microseconds. The fact that the measuring time (about 10-20 μs) is small compared to the characteristic time scale of most large-scale flow phenomena makes PIV a useful tool for the investigation of unsteady separated flow fields. Unsteady separated flow phenomena have received significant attention in recent developments of rotorcraft technology. In the case of a helicopter in high-speed forward flight for instance, the retreating rotor blades experience a combination of high incidences and low relative velocities of the oncoming freestream, so that an unsteady stalled flow field appears over a part of the blade as described previously. To be able to characterize the flow phenomena involved in this flight configuration the unsteady flow field has to be investigated. Flow visualization only yields qualitative information and also cannot resolve small-scale structures satisfactorily. As described above, numerical simulations have been performed in order to obtain instantaneous velocity fields, pressure distribution and lift, drag and moment data required for the design of the rotor blades. However, there are a few shortcomings, especially with regard to the simulation of the deep dynamic stall which is characterized by high pitching amplitudes and high reduced frequencies. Experimentally obtained instantaneous velocity data seem to be best suited as an input to improve numerical algorithms.

Most of these experimental results were obtained using flow visualization and pressure measurements. The periodic features of the velocity field over a pitching airfoil have also been explored by means of hot wires (Ref. 14) and most recently, by use of the Laser Doppler Anemometry (LDA) technique (Ref. 15). However, to study the mechanisms involved in such an unsteady flow, it would be advantageous to have instantaneous density field or instantaneous velocity field data. As explained above, a global method such as the Particle Image Velocimetry (PIV) technique is best suited to achieve the latter goal. The PIV technique was applied for the first time to a profile in a pitching up motion (Ref. 16). These experiments were conducted in a water towing tank at a Reynolds number of 5 000. The data are of high quality and show the details of boundary layer separation, formation and evolution of a vortex and the separation of the flow from the airfoil. However, experiments related to the problem of dynamic stall of rotor blades require oscillating motions at higher Reynolds numbers and therefore, have to be carried out in a wind tunnel. The investigations described in this paper are characterized by a Reynolds number based on chord length and freestream velocity of Re ~ 400 000.

Results and Discussion

NACA0012

1) Steady Results.

Figs. 3 include steady tangential as well as normal velocity profiles measured, (Ref.7), and calculated at 30% upper surface on the NACA0012 airfoil section. The results are obtained for a set of incidences: α=0deg/3deg/6deg/9deg/12deg. Fig. 2a includes calculations using the δ_2-transition onset criterion, Fig.2b is based on the δ'_3-criterion. Comparisons between experiment and calculation show that:

1.) The numerical data slightly under-predict the experiment. This holds for both tangential and normal velocities.

2.) The start of separation at α=12deg is not seen in the calculation; this effect may be attributed to the SA-turbulence model, which shows some insensitivity with respect to steady separation onset.

3.) The differences between the two transition onset methodologies based on δ_2 and δ'_3 show only small differences in the calculated data (Figs. 3a versus 3b).

2) Unsteady Results (Deep Dynamic Stall).

For the conventional NACA0012 airfoil section intensive experimental investigations during dynamic stall have been exercised and described in detail in Ref. 7.

The set of parameters used in the experimental study was:

Incidence variation	α = 12deg +- 6deg.cos (ωt)
Reynolds number	Re = 10^5
Reduced Frequency	k = 0.188
Mach number	M = 0.045 *)
Main velocity	U_∞ = 5m/s
Airfoil chord	c = 0.3m

*) The Mach number is a necessary input parameter for the numerical code and is set to a small number to simulate definitely incompressible flow.

In the following sequences of Figs. 4a-4g measured and calculated velocity profiles are displayed at three different chord wise

locations on the airfoil upper surface: x/c=0.3/0.5/0.67. The left figures include numerical results based on the δ_2 transition onset criterion, the right figures display the numerical results based on δ'_3.
During the up stroke motion the correspondence between calculation and experiment is good up to 16.24deg, see Fig.4c. Some smaller deviations occur for the δ'_3 criterion (right figure). Beyond 16deg up stroke the flow starts to separate and larger deviations between calculation and experiment are to be expected. At 16.24deg (Fig. 4c) negative velocities close to the airfoil surface are observed in the calculations but not in the data. In this case the separation bubble may be rather thin and therefore difficult to detect in the experiment. At 18deg maximum incidence (Fig. 4d) both calculation and experiment show strong backflow velocities in all three chord wise positions. The correspondence of the data with calculations based on δ_2 is somewhat better here. During the down stroke (Figs. 4d-g) the deviations are much larger. In the beginning of down stroke at 16.24deg (Fig. 4e) the calculations show thicker separation zones with a better fit to experiment with the δ'_3-criterion for transition onset. However in the following lower part of down stroke motion (Figs. 4f-g) the data show larger backflow velocities and more extended separation zones normal to the airfoil surface. In particular in the rear part (x/c=0.67) the differences are large, i.e. the reattachment process is shifted to smaller incidences.
It is difficult to judge for these strongly separated flows which transition criterion does a better job.

OA209

Fig.1 shows a sketch of the set up for 3D-measurements. Based on the experience achieved in the previous section and in particular based on numerical data it was decided to measure instantaneous boundary layer data for the two flow cases:

Light Dynamic Stall, α=6deg+-6deg.cos (ωt)
Deep Dynamic Stall, α=12deg+-6deg.cos (ωt)

with the reduced frequency k=0.188, Re=7x10^4.
In the experiments the three velocity components U (tangential), V (normal) to the airfoil surface and W (span-wise direction) have been measured for a phase-averaged period with steps of two degrees phase angle. The measurements have taken place at three different chord wise positions on the model upper surface, i.e. at x/c=0.05; x/c=0.10; x/c=0.25. Calculations as well as flow visualizations prior to these experiments have shown that at these positions reversed flow areas develop during the oscillatory cycle. From this information it may be possible to indirectly conclude on the development of transition during the cycle. Figs. 5-10 include the measured and calculated results for the Light Stall case. Figs. 11-16 include the corresponding data for the Deep Stall case.

1) Unsteady Results (Light Dynamic Stall).
In the light dynamic stall case the following parameters have been realized:

Incidence variation	α = 6deg +- 6deg.cos (ωt)
Reynolds number	Re = 0.7.10^5
Reduced Frequency	k = 0.188
Mach number	M = 0.045$^{*)}$
Main velocity	U_∞ = 5m/s
Airfoil chord	c = 0.2m

$^{*)}$ The Mach number is a necessary input parameter for the numerical code and is set to a small number to simulate definitely incompressible flow.
Figs. 5a (calculation) and 5b (measurement) show tangential velocity distributions U [m/s] versus phase (incidence) at different positions Y [mm] through the boundary layer or separated flow region at 25% chord upper surface. At Y=1.5mm calculation (Fig. 5a) shows only a small reversed flow area during down stroke. However closer to the airfoil surface (Y=0.36 and Y=0.69mm, dashed lines) the flow is reversed over parts of both up stroke and down stroke motion. The experimental results at Y=1.5mm only touch the zero line. Figs. 6a (complete velocity profile) and 6b (details close to the surface) show calculated and measured tangential velocities U versus Y. The experimental data are displayed as filled circles. The calculations are represented by solid lines of the same colour. The correspondence between calculation and experiment is reasonable. Details close to the surface where experimental data are not available show calculated reversed flow areas starting beyond α=7deg with maximum extension at the beginning of the down stroke.
At x/c=0.10 (Figs. 7a-7b) the phase variation of the U-velocity component shows quite good correspondences between calculation and experiment. At Y=1mm reversed flow occurs

short before (experiment) and after (calculation) the maximum incidence. Remarkable correspondence occurs between calculated and measured data (colours refer to corresponding curves). Fig. 8 shows again calculated and measured velocity profiles. A reversed flow region is developing here very close to the airfoil surface represented both by calculation and experiment.
Further up stream at x/c=0.05 (Figs. 9a and b) phase variations are shown again for the U-velocity component. The calculation shows very smooth curves indicating that transition does not reach this position during the complete cycle. Very close to the surface (Y=0.1mm) flow reversal occurs over part of the cycle. The experimental data show severe scatter at both Y=3mm and 3.5mm respectively. A corresponding behavior is detected for the velocity profiles in Fig. 10. Experimental data show a reversed zone off the surface (at about Y=3mm) which cannot be seen in the calculation.

2) Unsteady Results (Deep Dynamic Stall).
Figs. 11a and 11b show again calculated and measured phase variations of the U-velocity component at x/c=0.25. It is now obvious that calculated transition is reaching this position over a larger portion of the oscillatory cycle. Corresponding reversed flow areas occur beyond α=14deg up stroke to α=11deg down stroke. The experimental data show a similar behavior however the backflow velocities are larger. Fig. 12 includes again calculated and measured velocity profiles. Details in this plot show for the experiment that the start of separation does occur earlier in the loop and keeps this phase shift also during the down stroke motion. Figs. 13a and 13b show the flow situation at x/c=0.10. Calculated transition takes place over a considerable part of the up stroke extended into the down stroke to about α=10deg. The experimental curves show a remarkable similar behavior with the beginning of separation earlier in the loop, i.e. at about α=13deg. Calculated and measured velocity profiles are compared in Figs. 14a and 14b (details). Reversed areas are measured and calculated at the same positions with reversed velocities of the same order of magnitude. The calculations show details of the start of flow reversal very close to the surface where measurement is not possible.
Figs. 15a and 15b show phase variations of U at x/c=0.05. The calculated curves still show transition between about α=13deg up stroke and α=15^o down stroke. At the relatively large distance of Y=3mm from the wall used in the experiment the calculation does not show reversed flow. However if the distance is reduced to 1mm (see Fig. 15a) flow regions of revered flow occur also in the calculation with considerable scatter which again must be attributed to the development of transition. Not very much correspondence is achieved for the velocity profiles displayed in Figs. 16a and 16b (details). Reversed flow has been measured also at this position close to the airfoil leading edge, but the flow minima are shifted away from the wall to larger Y-positions. The calculations also show backflow but much closer to the surface. Some further investigations should be undertaken to clear these discrepancies which have also been found in the Light Stall case.

3) PIV Investigations (Deep Dynamic Stall).
This part will present one of the first set of results obtained at LABM with the DANTEC PIV System. In the deep dynamic stall case the following parameters have been realized:

Incidence variation	α = 11deg +- 6deg.cos (ωt)
Reynolds number	Re = $0.7.10^5$
Reduced Frequency	k = 0.188
Mach number	M = 0.045$^{*)}$
Main velocity	U_∞ = 5m/s
Airfoil chord	c =0.2m

Readers may note that (x-y) axis is given in the camera frame and both origins characterize the quarter chord axis of the airfoil.
Figs. 17a to 17g (respectively 18a to 18g) show the absolute velocity (U/U_∞) evolution for different angle of attack during a pitching-up motion (respectively pitching-down). In general, a sub velocity at the leading edge of the airfoil is highlighted and due to the acceleration of the flow in this area. Moreover, this area increases with the value of α because negative pressure gradients are more and more important. On Figures 17a to 17g and 18a to 18g, blue area characterizes the presence of a laminar separation bubble which moves from the trailing edge (low value of α) to the leading edge (high value of α) of the airfoil. After that, the bubble is blocked at the leading edge, has more and more energy (due to the increase of α) and dynamic stall occurs thanks to the bursting of the bubble. Fig. 17g shows a little separation zone for α=16.266deg (up stroke) whereas Fig. 18g highlights a very important one for α=16.167deg (down stroke) which characterized a deep dynamic stall process during pitching down motion. The reattachment process begins from the leading

edge to the trailing edge according to Figs. 18g to 18a. Results presented here are in good agreement with those obtained in previous part (instantaneous velocity profiles and tangential velocity profile versus phase at x/c=0.25 and 0.10).
Figs. 19a to 19g (respectively 20a to 20g) show the local vorticity (Ω) evolution for different angle of attack during a pitching-up motion (respectively pitching-down). On these Figures, the 3D vortical flow structures emitted in the vicinity of the airfoil boundary layer are highlighted with their vorticity. Figs. 19a show the evolution of the vorticity along the airfoil chord for α=6.401deg due to the vortex shedding phenomena. Indeed, there are more and more vortex when α increases (Figs 19d, 19e, 19f) whereas their vorticity decreases when they are convected in the wake. During up stroke motion, there are less vortex in the wake of the airfoil (Figs. 19a to 19g) compared to the down stroke motion. Indeed, in this last case, Figs. 20a to 20g show the presence of multiple 3D vortical flow structures due to the reattachment process which occurs after a deep dynamic stall which is synonymous of a very high turbulent flow in the wake of the airfoil. Moreover, pitching up motion is characterized by clockwise vortex (Figs. 19b, 19d, 19f, 19g) due to the roll up of the shear stress layer whereas during pitching down motion, clockwise and counter clockwise vortex are highlighted (Figs. 20d, 20f, 20g).

Conclusions

Numerical and experimental investigations have been carried out for two different airfoil sections:

1) NACA0012
2) OA209

to investigate the complex flow about the oscillating airfoil at both light and deep dynamic stall conditions.
A time accurate numerical code based on the full equations has been used for the numerical part of the investigations. The Spalart-Allmaras one-equation turbulence model has been used for these calculations. Two different transition onset methodologies have been applied in the present investigation: A transition onset model based on Michel's criterion with the momentum loss thickness as basis and a model based on the energy loss thickness. The following transition zone is calculated in both cases by means of the Chen-Tyson exponential growth model. The results from both models show some typical differences in the sense that the model based on the energy loss thickness predicts the transition onset point more up stream. Detailed future experiments are necessary to clear the situation which model gives the more appropriate physical answer.
On the experimental side different measurement techniques have been applied:

1) Embedded LDV (ELDV) technique to measure instantaneous velocity profiles along the airfoil at the same positions relative to the moving airfoil surface,
2) Particle Image Velocimetry (PIV) along the airfoil upper surface during its oscillatory motion.

Extensive PIV-measurements have been made in the LABM small size wind tunnel facility and the first set of experiments is quite satisfactory and is in good agreement with velocity profiles results obtained thanks to ELDV and Navier-Stokes numerical code.

Acknowledgements

The authors are particularly thankful to the SPI Department of CNRS which partly supported this collaborative work between DLR and LABM.

References

1- W. GEISSLER, G. DIETZ, H. MAI, B. JUNKER, T. LORKOWSKI, "Dynamic Stall Control Investigations on a Full Size Chord Blade Section", 30th European Rotorcraft Forum, 14.-16.9.2004, Marseille, France.

2- W. GEISSLER, L.W. CARR, M.S. CHANDRASEKHARA, M.C. WILDER, H. SOBIECZKY, "Compressible Dynamic Stall Calculations Incorporating Transition Modeling For Variable Geometry Airfoils",36th AIAA Aerospace Meeting and Exhibit, Reno Hilton, Reno, NV, January, 12-15, 1998.

3- W. GEISSLER, Instationäres Navier-Stokes Verfahren für beschleunigt bewegte Profile mit Ablösung (Unsteady Navier-Stokes Code for Accelerated Moving Airfoils with Separation) in German, DLR-FB 92-03, 1992.

4- K.K. CHEN, N.A. THYSON, "Extension of Emmons's Spot Theory to Flow on Blunt Bodies", AIAA J., Vol.9, pp.821-825, 1971.

5- R. MICHEL, "Etude de la transition sur les Profits d'Aile: Etablissement d'un Profil Incompressible, ONERA Dept 1/1578A, 1951.

6- W. GEISSLER, M.S. CHANDRASEKHARA, M.F. PLATZER, L.W. CARR, "The Effect of Transition Modelling on the Prediction of

Compressible Deep Dynamic Stall", 7th Asian Congress of Fluid Mechanics, Madras, India, Dec. 8-12 1997.

7- C. ALLAIN, "Contribution à l'étude expérimentale de la couche limite soumise à une instationnarité forcée. Application aux phénomènes de transition et de décollement en écoulement instationnaire 2D/3D", Thèse de Doctorat de l'Université Aix-Marseille II, 2001.

8- . BERTON, D. FAVIER, M. NSI MBA, C. MARESCA, C. ALLAIN, "Embedded LDV measurements methods applied to unsteady flow investigation", Experiments in Fluids, Vol. 30, N°1, pp.102-110, 2001.

9- E. BERTON, D. FAVIER, C. MARESCA, "Experimental and numerical investigation of dynamic stall at IRPHE/ASI Laboratory", 24th European Rotorcraft Forum, Cheeseman Award Presentation, Marseille 1998.

10- C. MARESCA, E. BERTON, D. FAVIER, A. BENYAHIA, "Study of 2D and 3D boundary layer of moving walls by embedded LDV measurements" Final Technical Report N° 68171-01-M-5090, ERO of the US Army, March 2002.

11- R. BEAM, R.F. WARMING, "An Implicit Factored Scheme for the Compressible Navier-Stokes Equations" , AIAA J.,Vol.6,No.4 April 1978.

12- P.R. SPALART, S.R. ALLMARAS, "A One Equation Turbulence Model for Aerodynamic Flows", AIAA-paper 92-0439, January 1992.

13- F.R. MENTER, "Improved Two-Equation k-ω-Turbulence Models for Aerodynamic Flows", NASA TM-103975, October 1992.

14- J. DE RUYCK, C. HIRSCH, "Instantaneous Flow Field Measurements of Stalled Regions on an Oscillating Airfoil", AIAA 17th Fluid Dynamics, Plasma Dynamics, and Lasers Conference, Snowmass, Colorado, USA, AIAA paper 84-1565, 1984.

15- M.S. Chandrasekhara and S. Ahmed, "Laser Velocimetry Measurements of Oscillating Airfoil Dynamic Stall Flow Field", AIAA Paper 91-1799, Honolulu, HI, Jun. 1991.

16- C. SHIH, A. KROTHAPALLI, S. GOGINENI, "Experimental Observations of Instability modes in a Rectangular Jet", AIAA Journal, 30-10, pp.2388-2394, 1992.

Figures

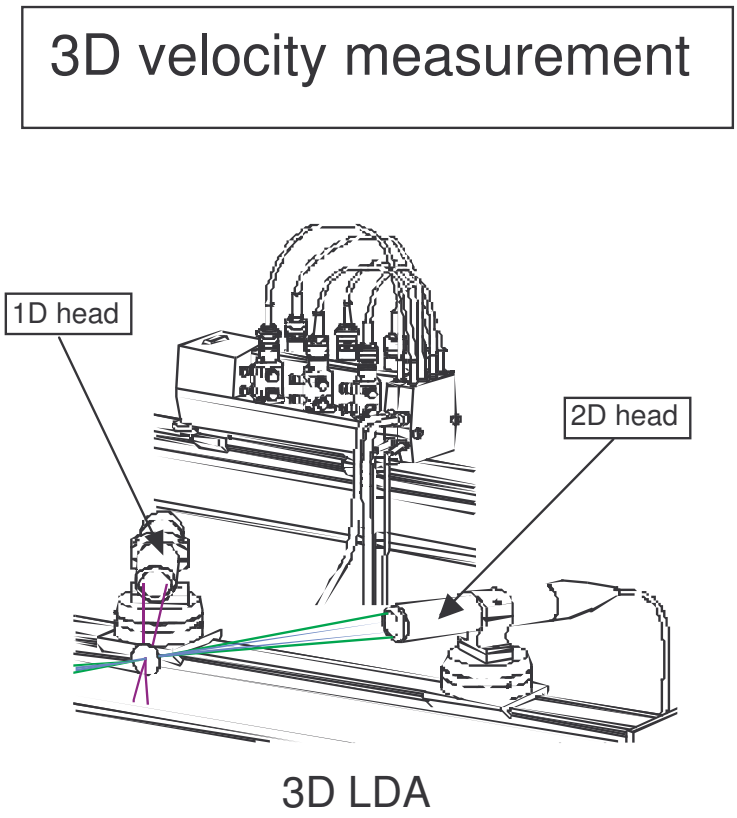

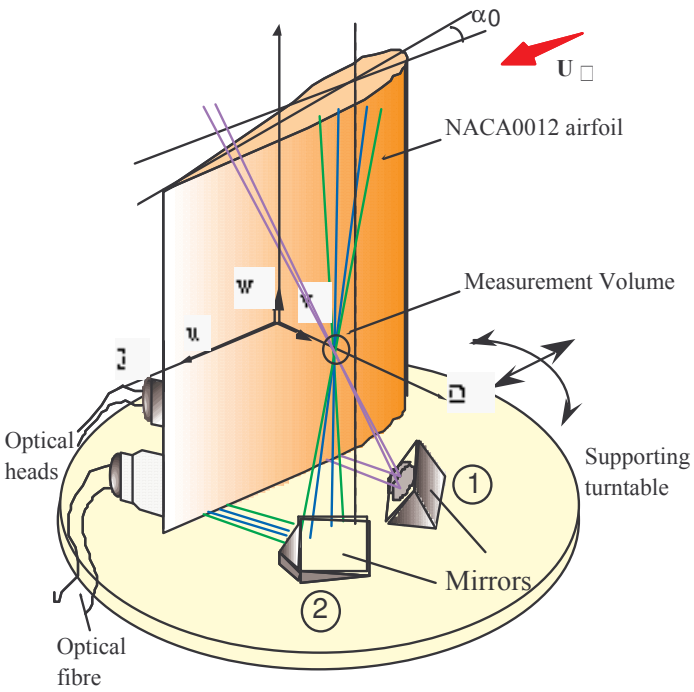

Fig. 1: 3D LDA Test Set-Up.

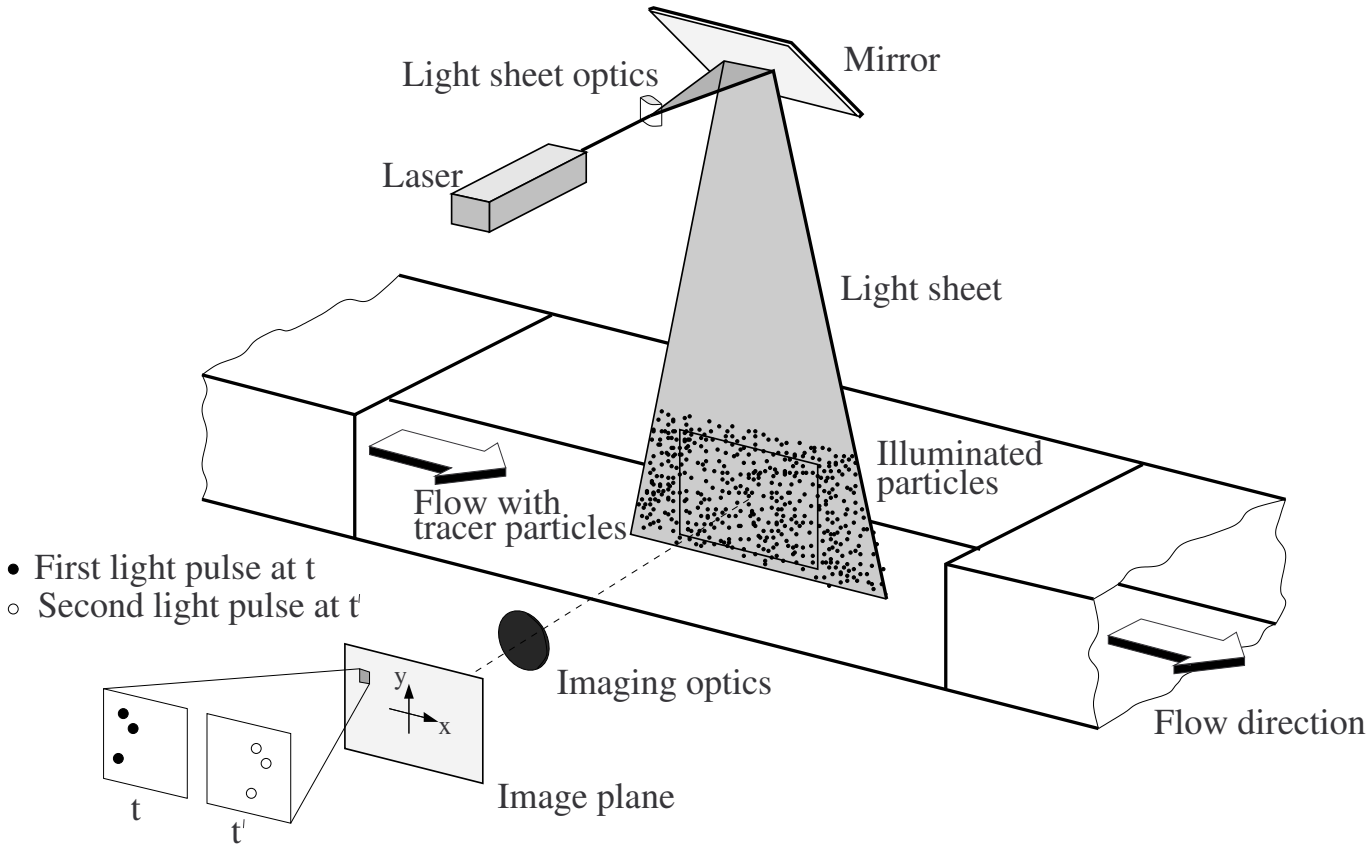

Fig. 2: 2D PIV Test Set-up.

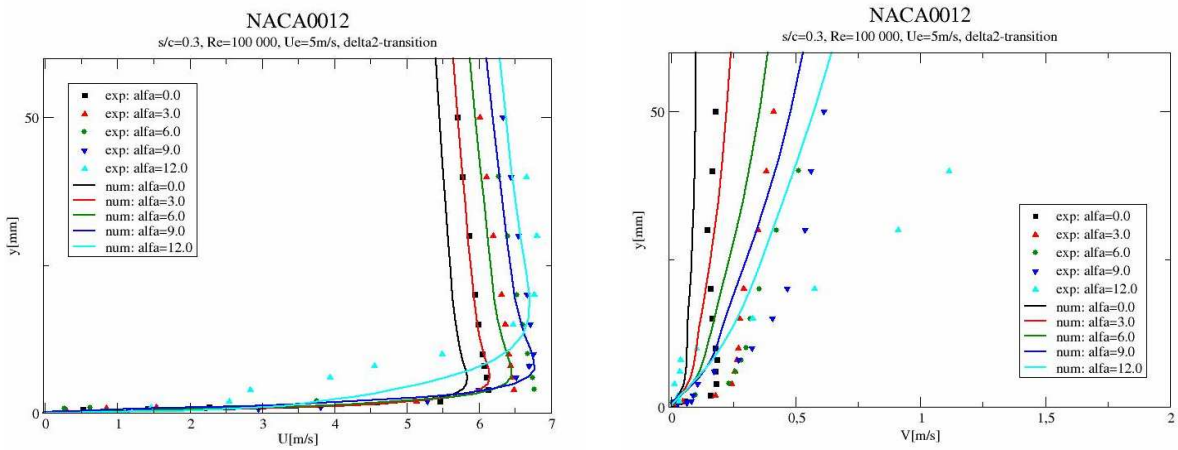

Fig. 3a: Steady Calculated and Measured Velocity Profiles at 30% Upper Surface. Tangential Velocities (left), Normal Velocities (right); δ_2 -transition onset criterion.

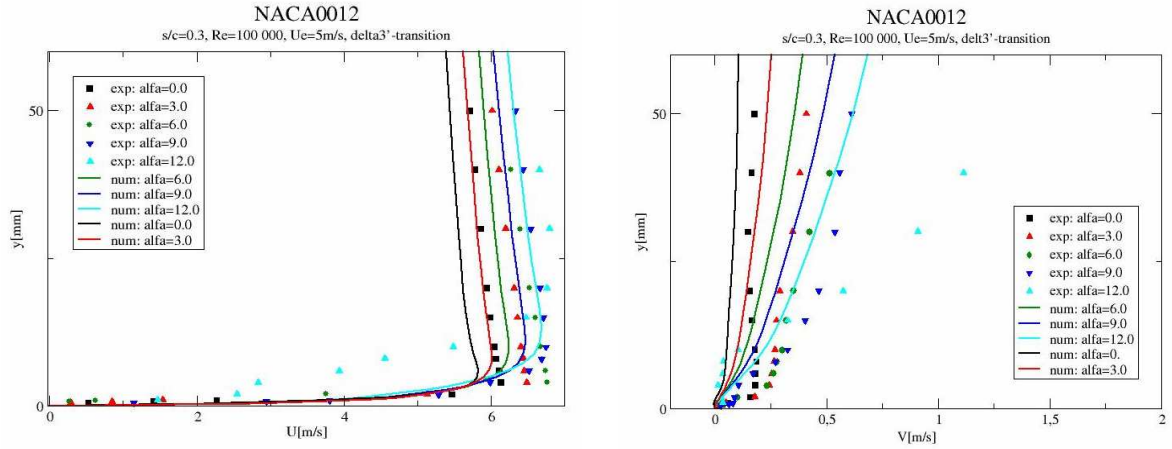

Fig. 3b: Steady Calculated and Measured Velocity Profiles at 30% Upper Surface. Tangential Velocities (left), Normal Velocities (right); δ_3' -transition onset criterion.

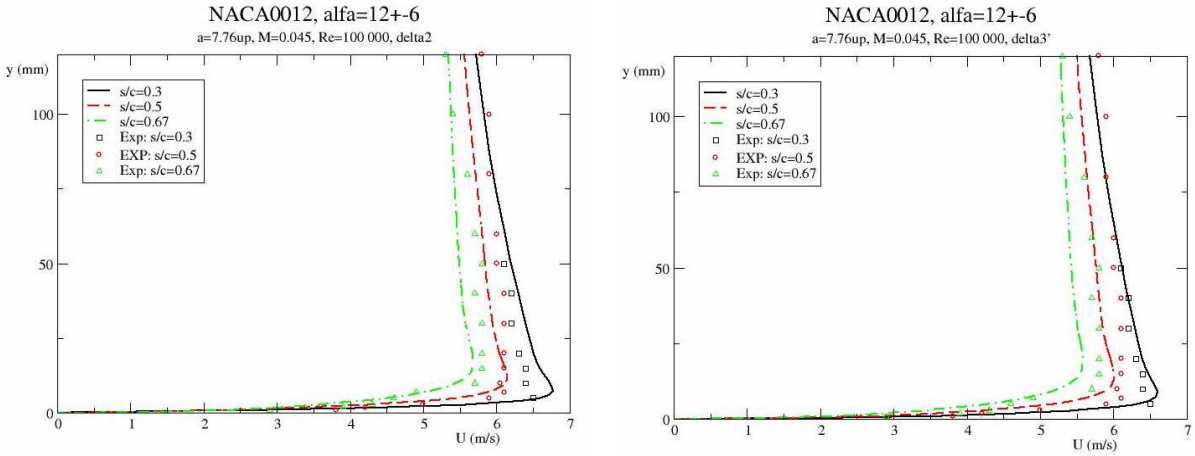

Fig. 4a: Measured and Calculated Velocity Profiles at α=7.76deg up stroke, Transition-Onset with δ_2 (left), with δ_3' (right).

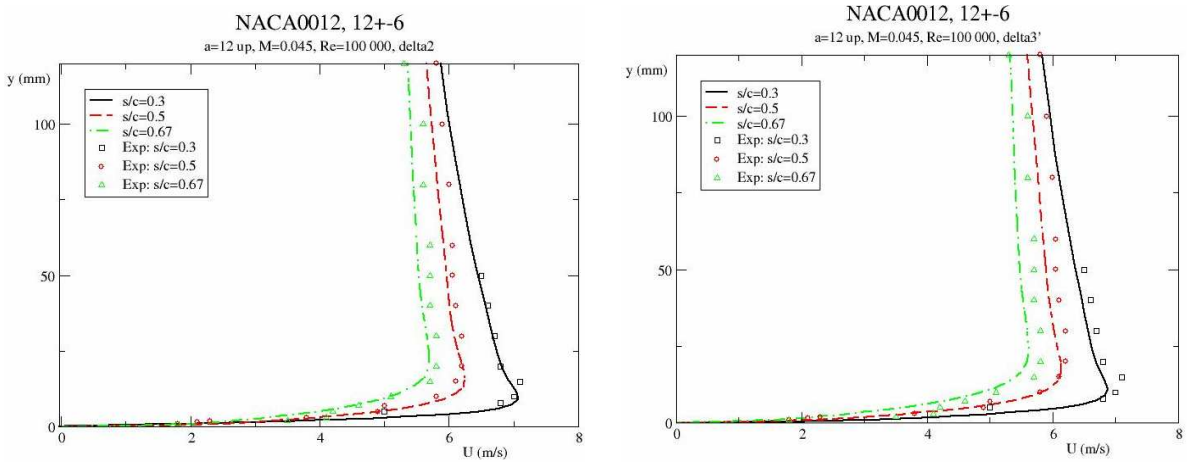

Fig. 4b: Measured and Calculated Velocity Profiles at α=12.0deg up stroke, Transition-Onset with δ_2 (left), with δ_3' (right)

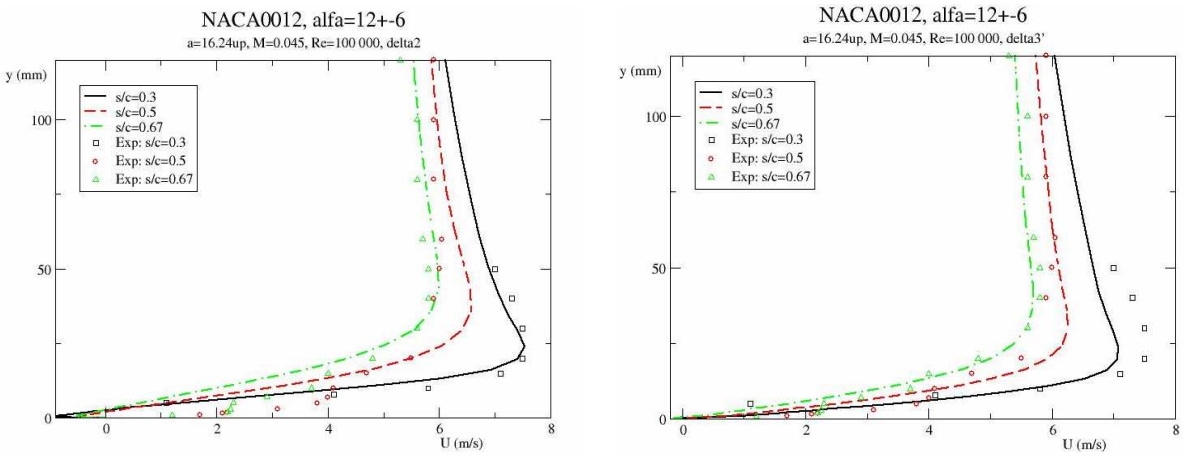

Fig. 4c: Measured and Calculated Velocity Profiles at α=16.24deg up stroke, Transition-Onset with δ_2 (left), with δ_3' (right)

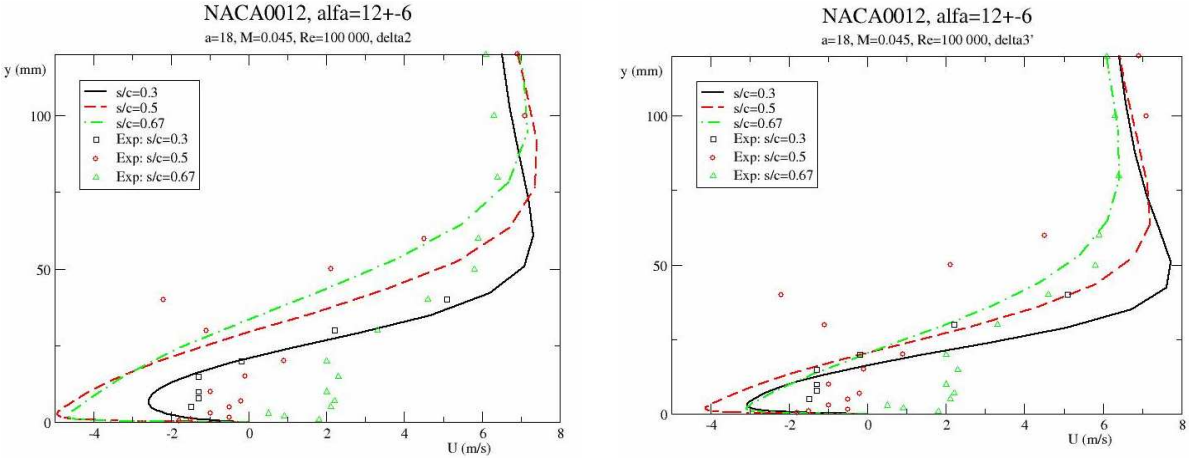

Fig. 4d: Measured and Calculated Velocity Profiles at α=18.0deg , Transition-Onset with δ_2 (left), with δ_3' (right)

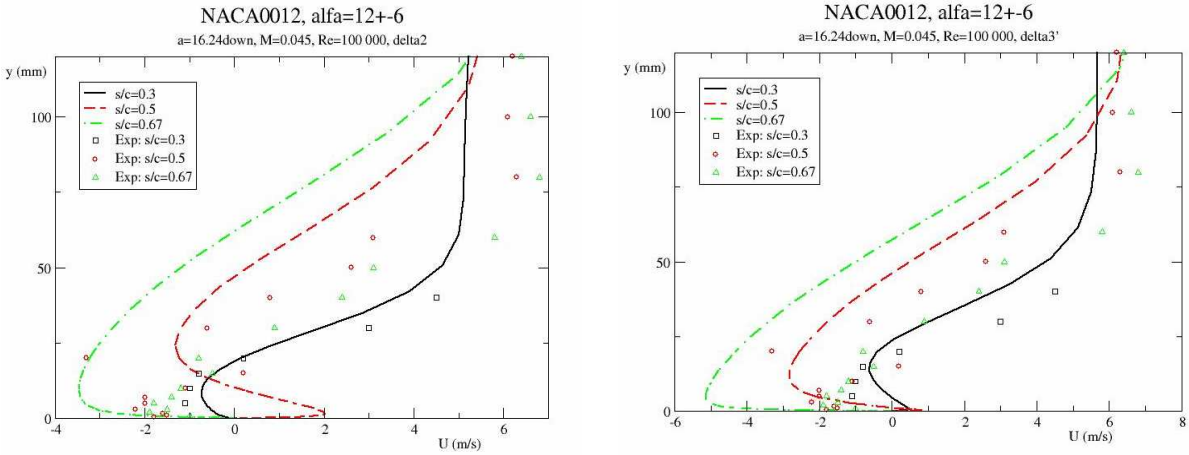

Fig. 4e: Measured and Calculated Velocity Profiles at α=16.24deg down stroke, Transition-Onset with δ_2 (left), with δ_3' (right)

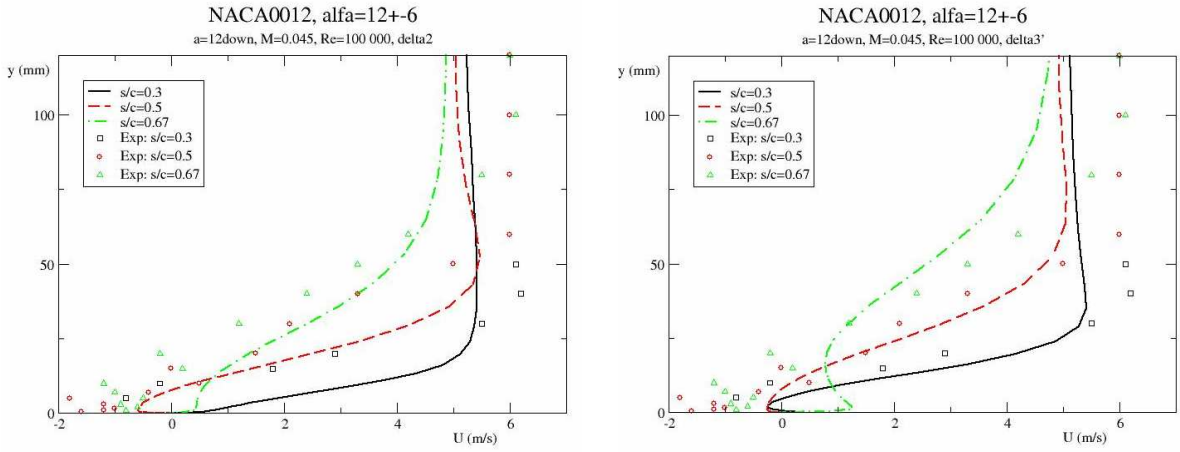

Fig. 4f: Measured and Calculated Velocity Profiles at α=12.0deg down stroke, Transition-Onset with δ_2 (left), with δ_3' (right)

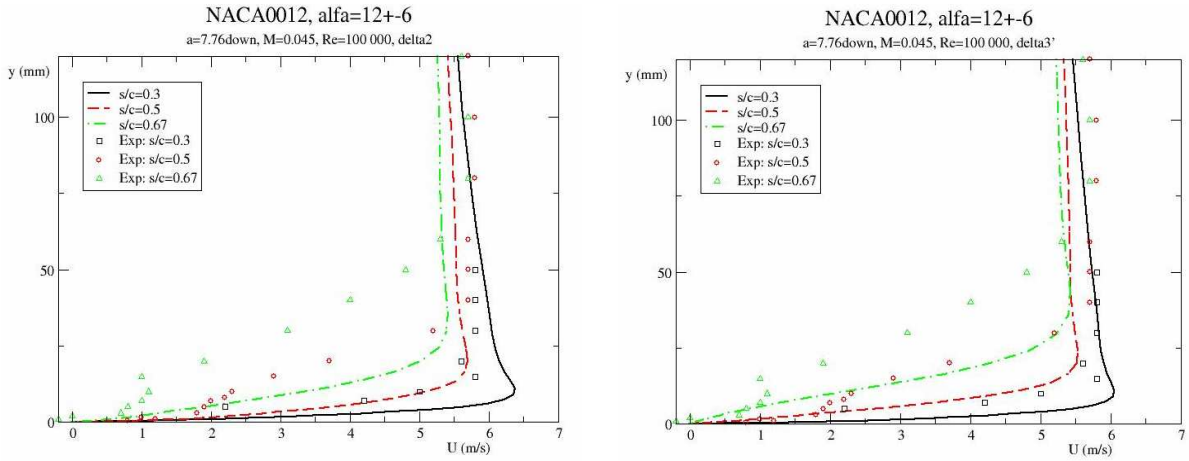

Fig. 4g: Measured and Calculated Velocity Profiles at α=7.76deg down stroke, Transition-Onset with δ_2 (left), with δ_3' (right)

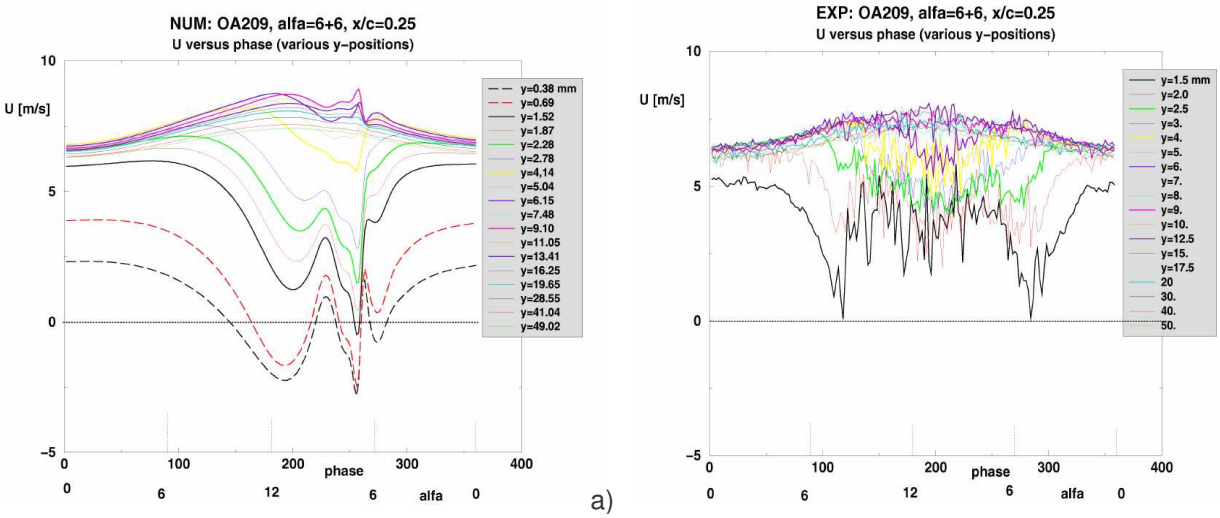

a) b)

Fig. 5: Tangential Velocities versus Phase (Incidence) at different Locations through the Boundary Layer; a) Numerical Calculations, b) Experiments at Light Stall, x/c=0.25.

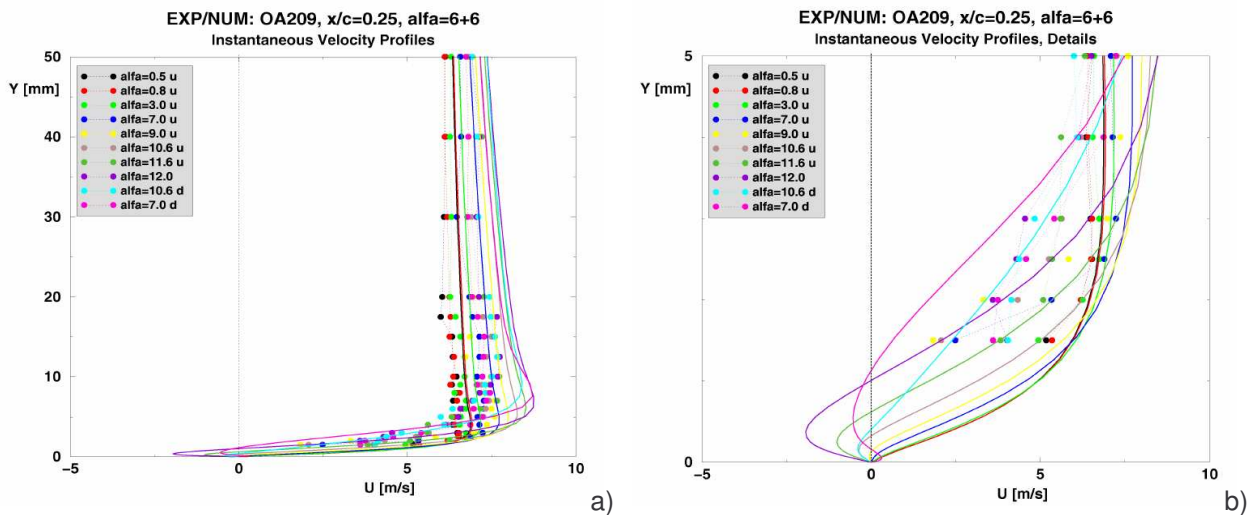

a) b)

Fig. 6: Instantaneous Velocity Profiles at Selected Incidences;
Comparison: a) Calculation/ Experiment, b) Details Close to the Wall at Light Stall, x/c=0.25.

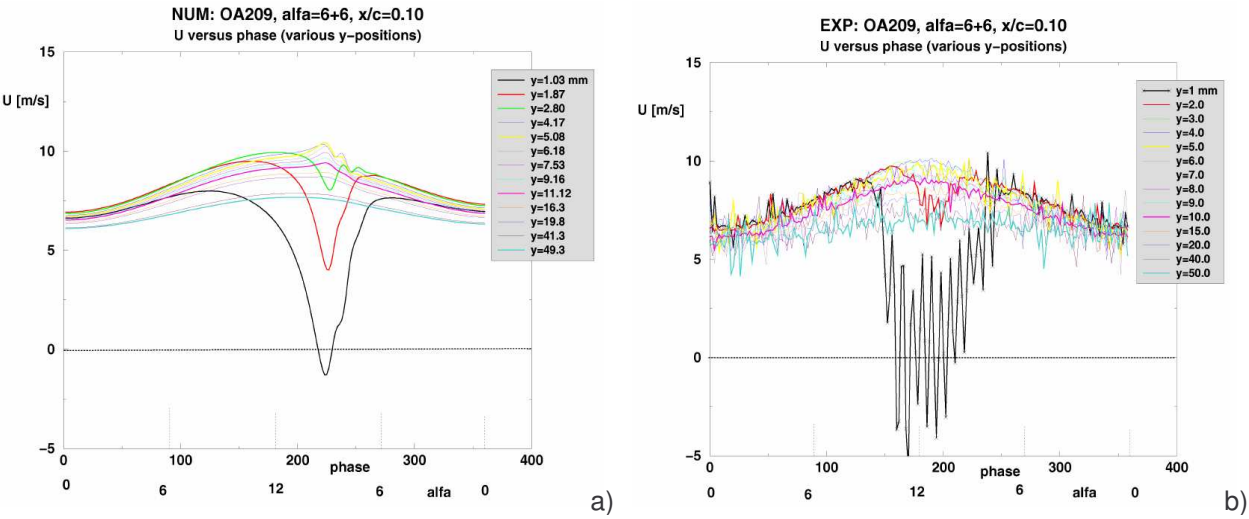

a) b)

Fig. 7: Tangential Velocities versus Phase (Incidence) at different Locations through the Boundary Layer; a) Numerical Calculations, b) Experiments at Light Stall, x/c=0.10.

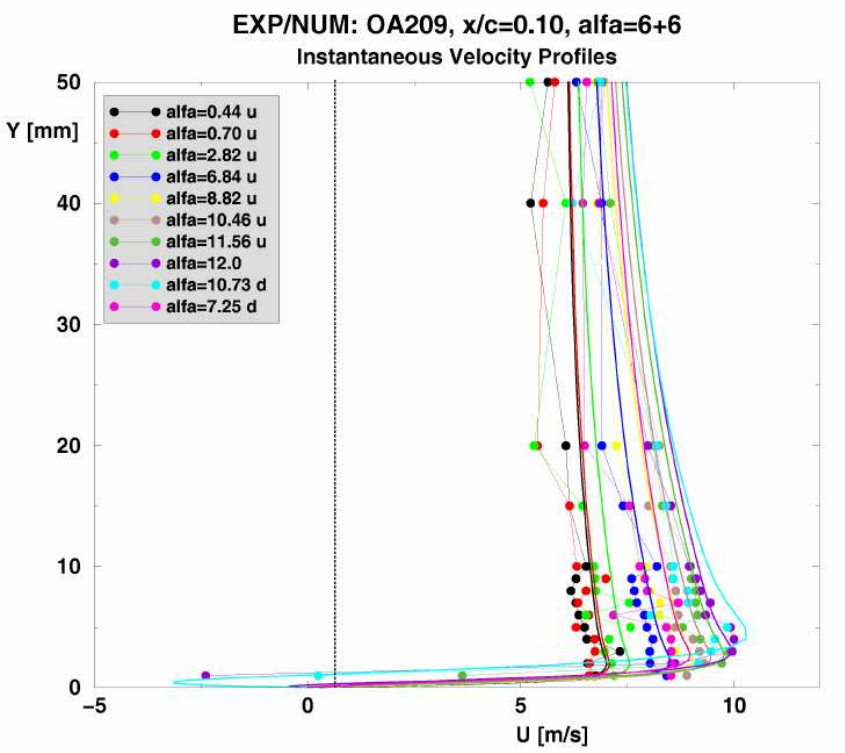

Fig. 8: Instantaneous Velocity Profiles at Selected Incidences; Comparison: Calculation/ Experiment at Light Stall, x/c=0.10.

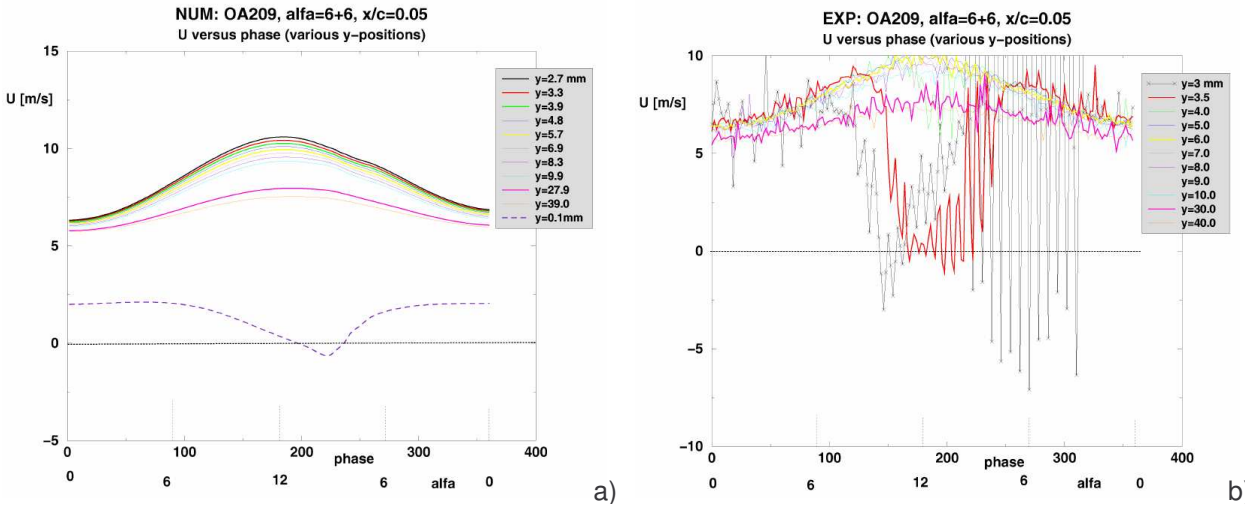

a) b)

Fig. 9: Tangential Velocities versus Phase (Incidence) at different Locations through the Boundary Layer; a) Numerical Calculations, b) Experiments at Light Stall, x/c=0.05.

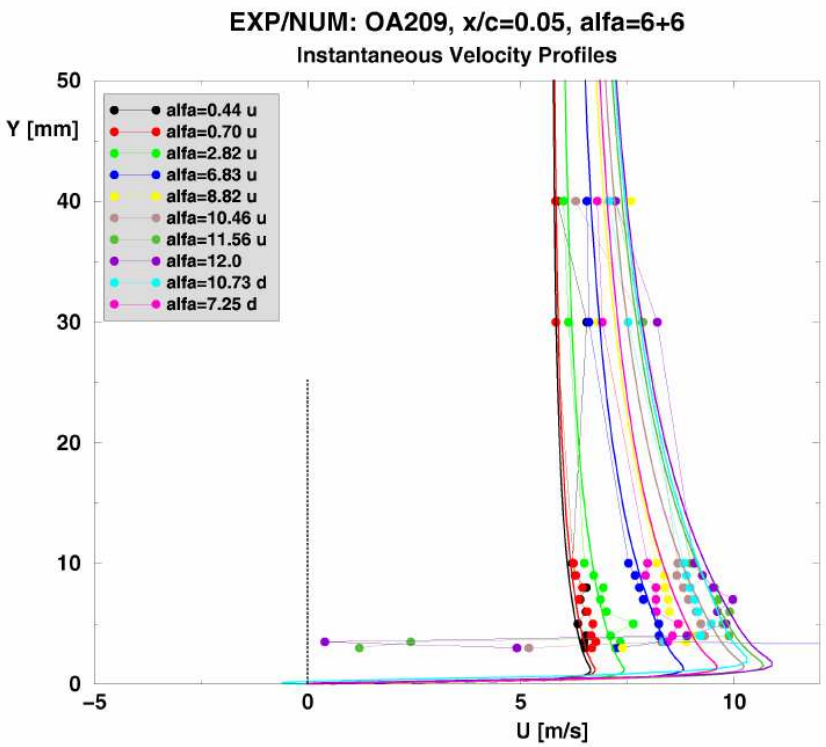

Fig. 10: Instantaneous Velocity Profiles at Selected Incidences; Comparison: Calculation/ Experiment at Light Stall, x/c=0.05.

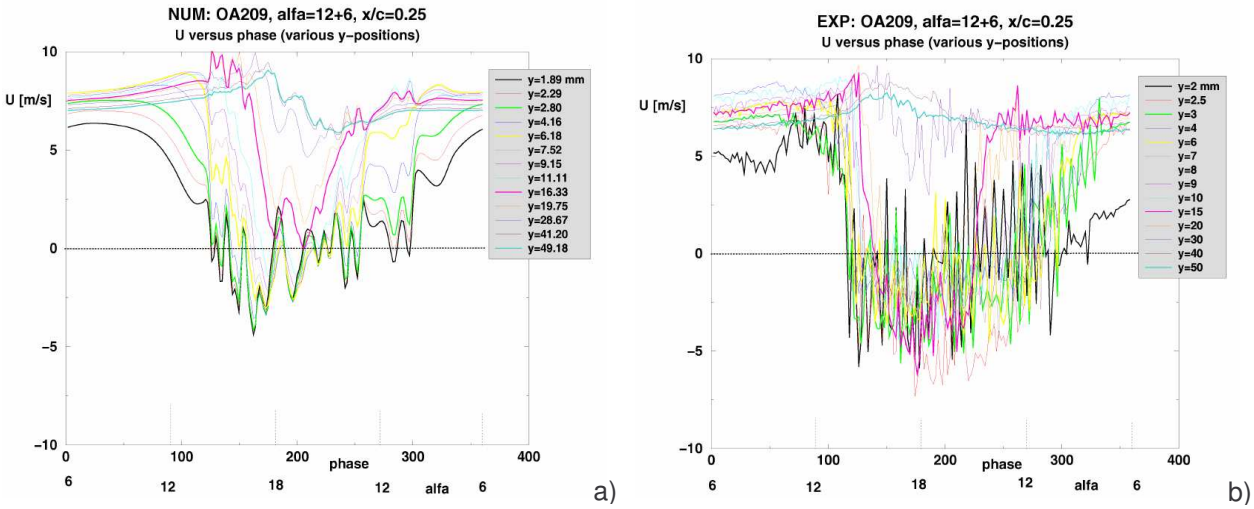

a) b)

Fig. 11: Tangential Velocities versus Phase (Incidence) at different Locations through the Boundary Layer; a) Numerical Calculations, b) Experiments at Deep Stall, x/c=0.25.

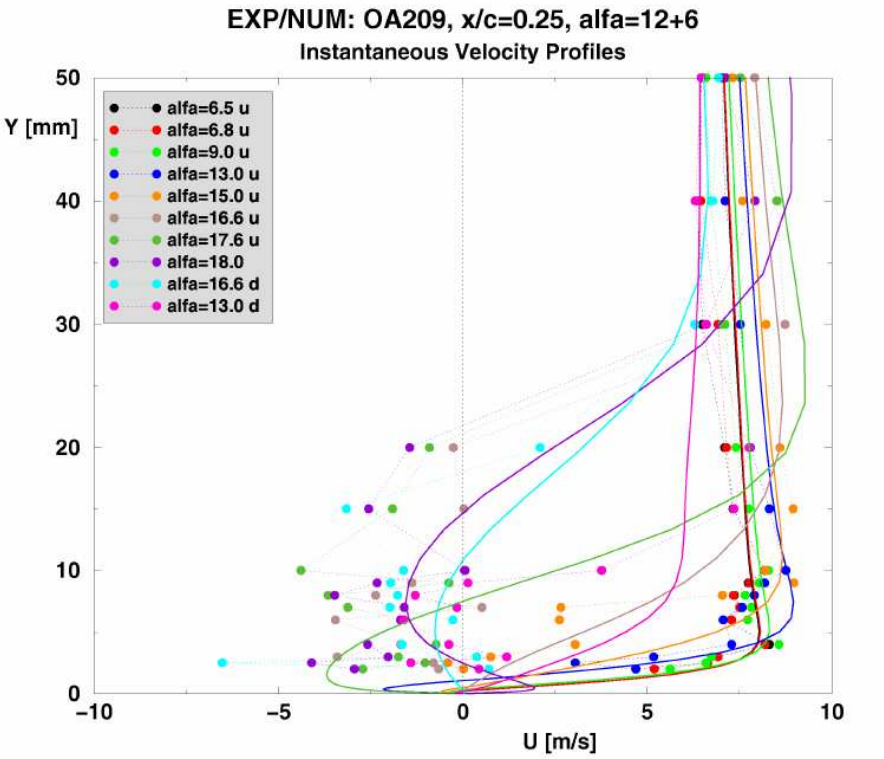

Fig. 12: Instantaneous Velocity Profiles at Selected Incidences; Comparison: Calculation/ Experiment at Deep Stall, x/c=0.25.

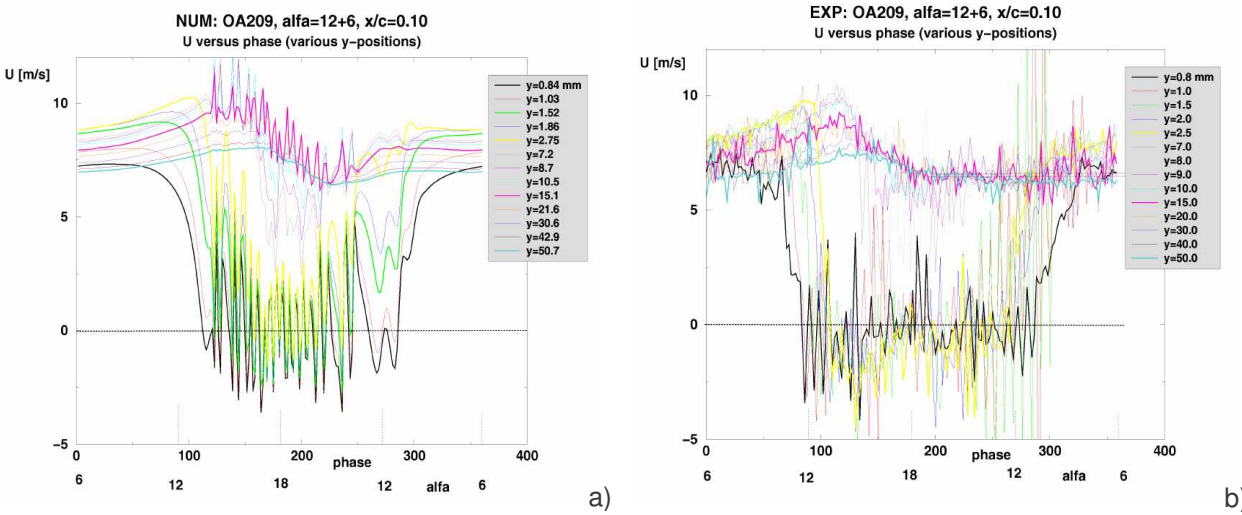

a) b)

Fig. 13: Tangential Velocities versus Phase (Incidence) at different Locations through the Boundary Layer; a) Numerical Calculations, b) Experiments at Deep Stall, x/c=0.10.

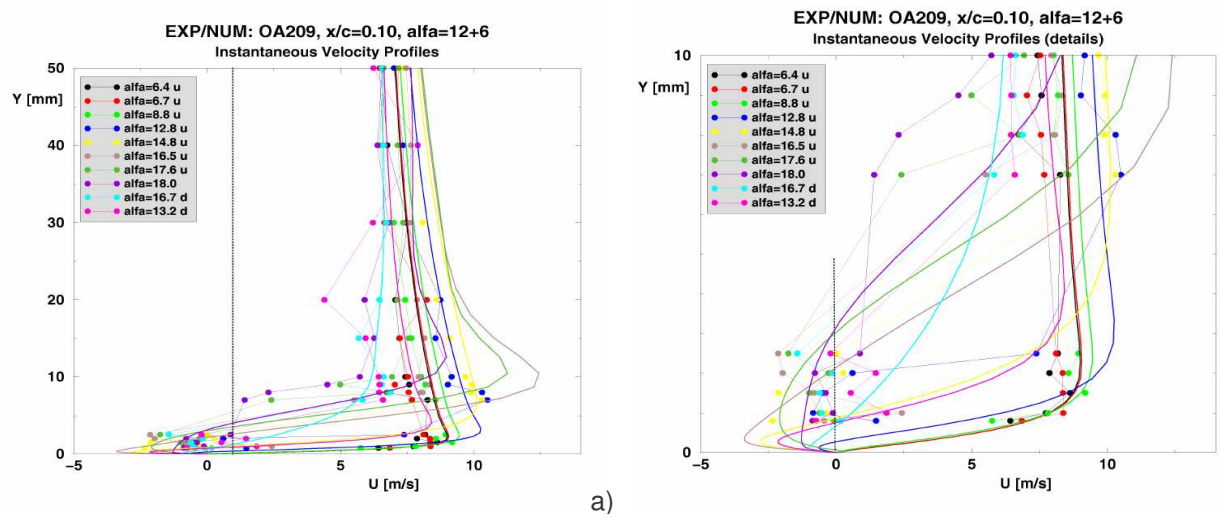

a) b)

Fig. 14: Instantaneous Velocity Profiles at Selected Incidences;
Comparison: a) Calculation/ Experiment, b) Details Close to the Wall at Deep Stall, x/c=0.10.

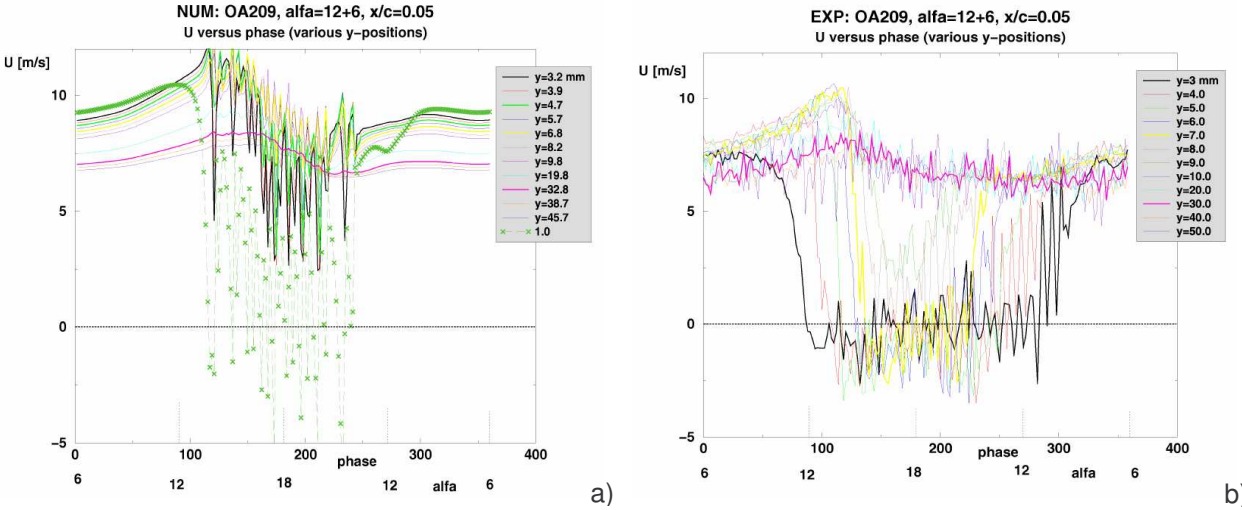

a) b)

Fig. 15: Tangential Velocities versus Phase (Incidence) at different Locations through the Boundary Layer; a) Numerical Calculations, b) Experiments at Deep Stall, x/c=0.05.

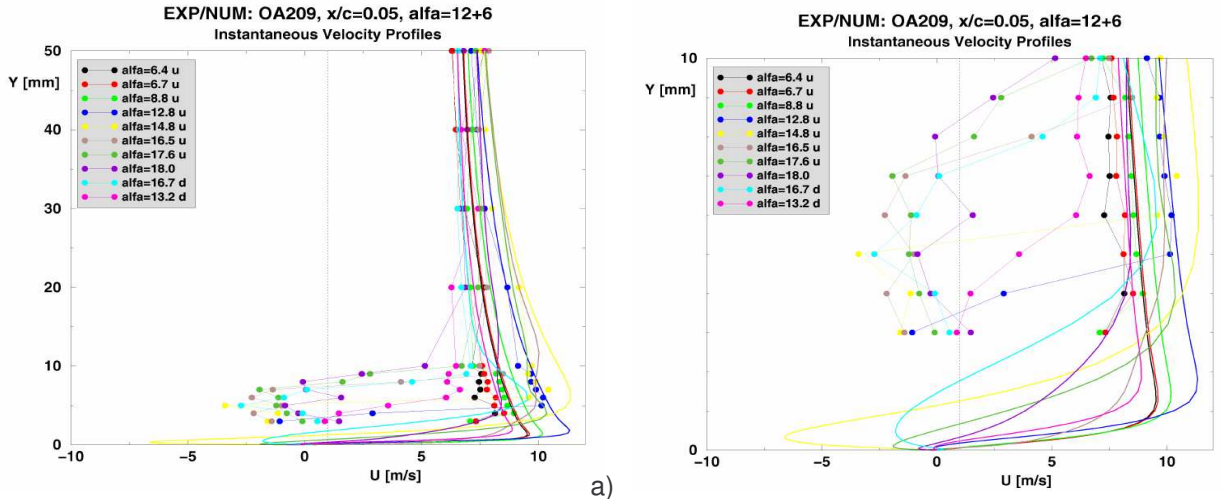

a) b)

Fig. 16: Instantaneous Velocity Profiles at Selected Incidences;
Comparison: a) Calculation/ Experiment, b) Details Close to the Wall at Deep Stall, x/c=0.05.

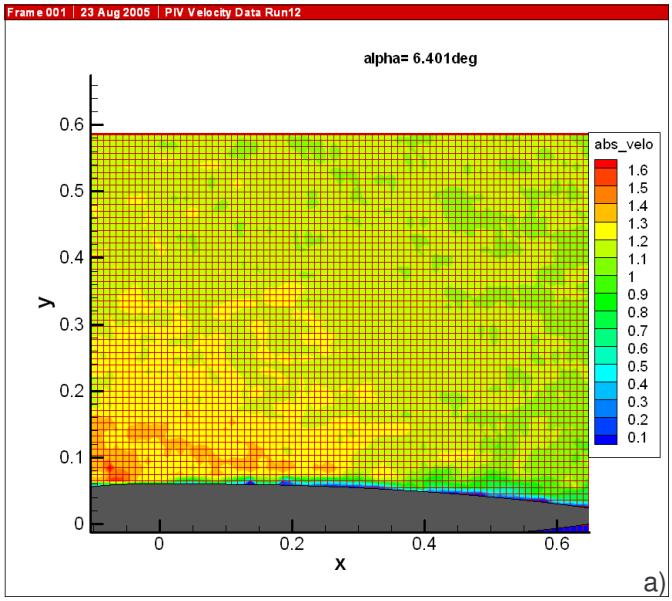
Frame 001 | 23 Aug 2005 | PIV Velocity Data Run12
alpha= 6.401deg
abs_velo
1.6
1.5
1.4
1.3
1.2
1.1
1
0.9
0.8
0.7
0.6
0.5
0.4
0.3
0.2
0.1
y
x
0
0.1
0.2
0.3
0.4
0.5
0.6
a)

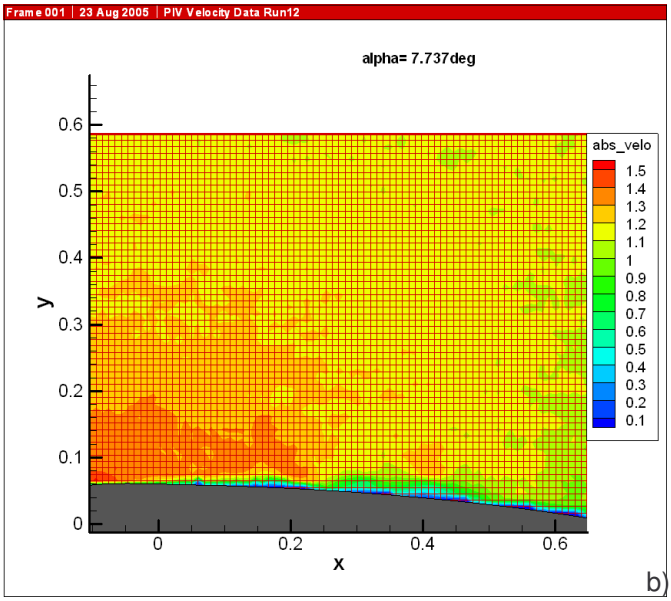
Frame 001 | 23 Aug 2005 | PIV Velocity Data Run12
alpha= 7.737deg
abs_velo
1.5
1.4
1.3
1.2
1.1
1
0.9
0.8
0.7
0.6
0.5
0.4
0.3
0.2
0.1
y
x
0
0.1
0.2
0.3
0.4
0.5
0.6
b)

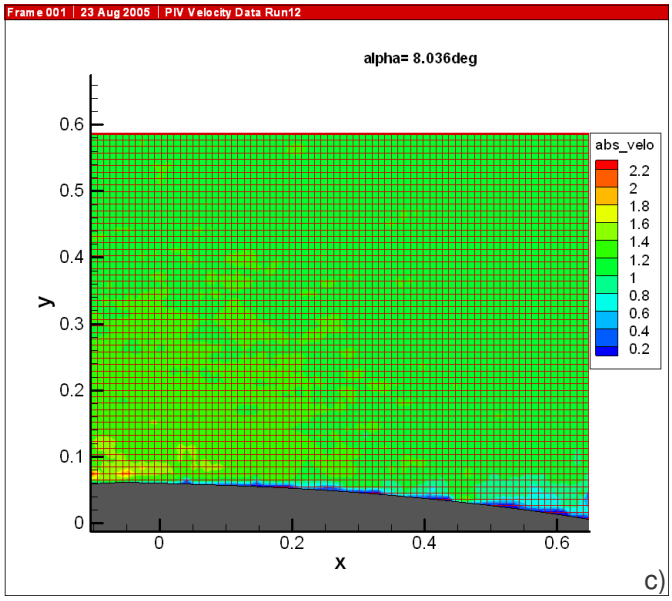
Frame 001 | 23 Aug 2005 | PIV Velocity Data Run12
alpha= 8.036deg
abs_velo
2.2
2
1.8
1.6
1.4
1.2
1
0.8
0.6
0.4
0.2
y
x
0
0.1
0.2
0.3
0.4
0.5
0.6
c)

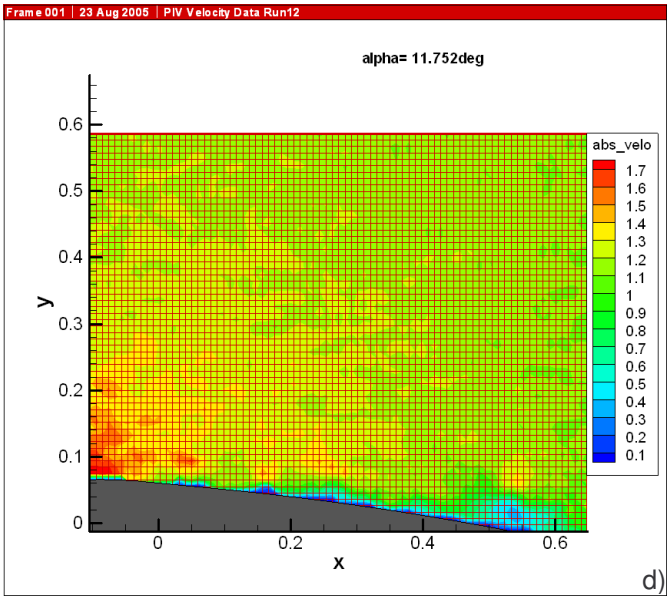
Frame 001 | 23 Aug 2005 | PIV Velocity Data Run12
alpha= 11.752deg
abs_velo
1.7
1.6
1.5
1.4
1.3
1.2
1.1
1
0.9
0.8
0.7
0.6
0.5
0.4
0.3
0.2
0.1
y
x
0
0.1
0.2
0.3
0.4
0.5
0.6
d)

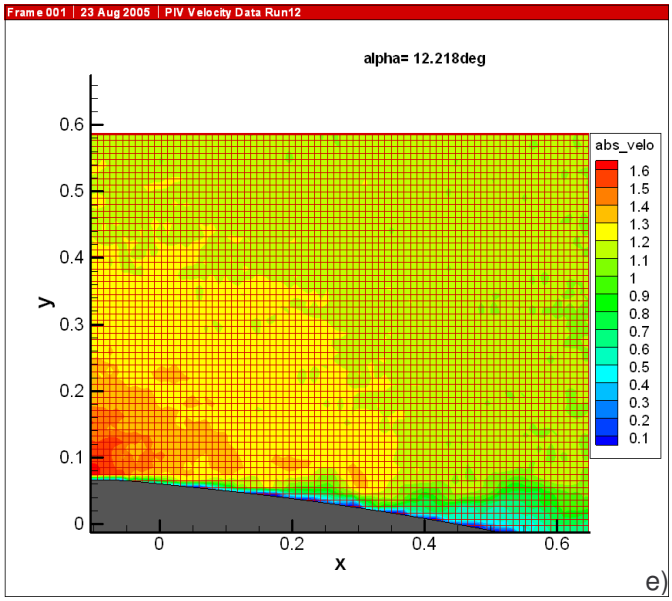
Frame 001 | 23 Aug 2005 | PIV Velocity Data Run12
alpha= 12.218deg
abs_velo
1.6
1.5
1.4
1.3
1.2
1.1
1
0.9
0.8
0.7
0.6
0.5
0.4
0.3
0.2
0.1
y
x
0
0.1
0.2
0.3
0.4
0.5
0.6
e)

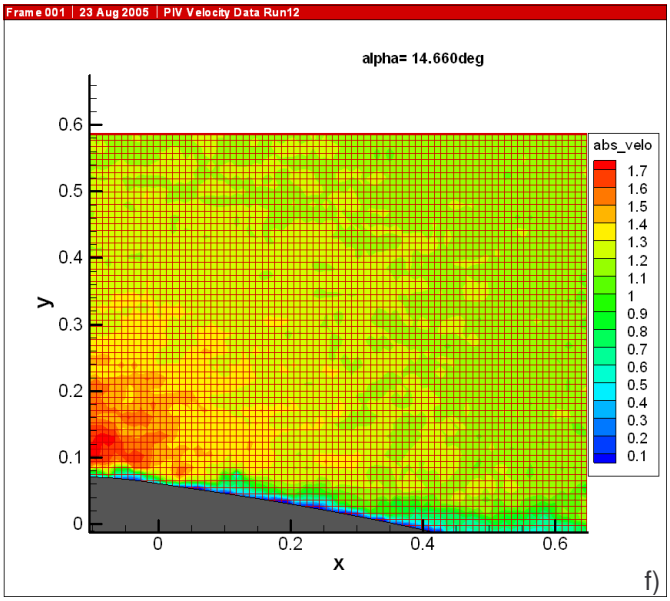
Frame 001 | 23 Aug 2005 | PIV Velocity Data Run12
alpha= 14.660deg
abs_velo
1.7
1.6
1.5
1.4
1.3
1.2
1.1
1
0.9
0.8
0.7
0.6
0.5
0.4
0.3
0.2
0.1
y
x
0
0.1
0.2
0.3
0.4
0.5
0.6
f)

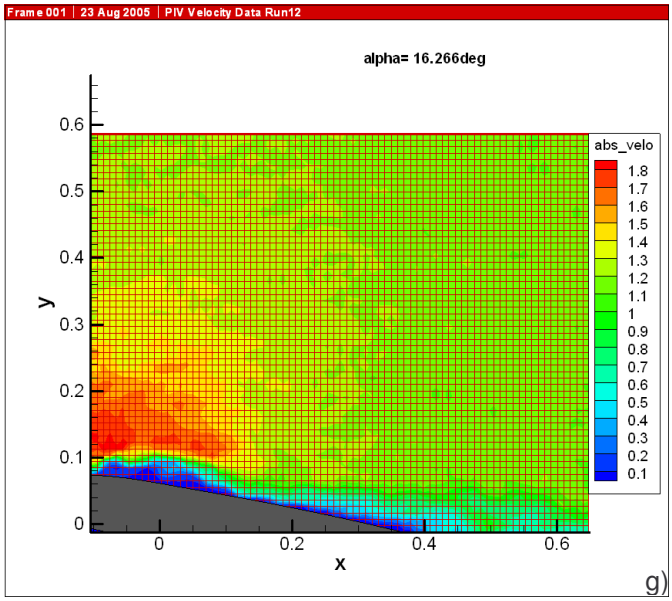

Fig. 17: Absolute velocity U/U_∞ evolution during up stroke motion for α (t) =11deg+-6deg.

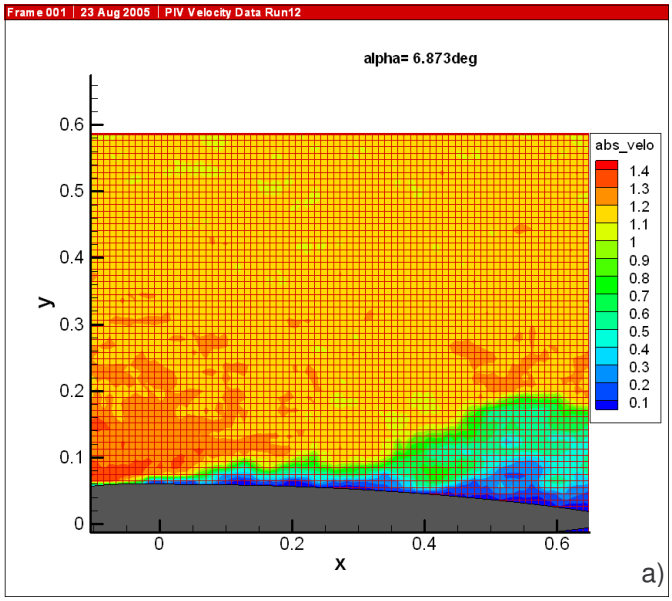

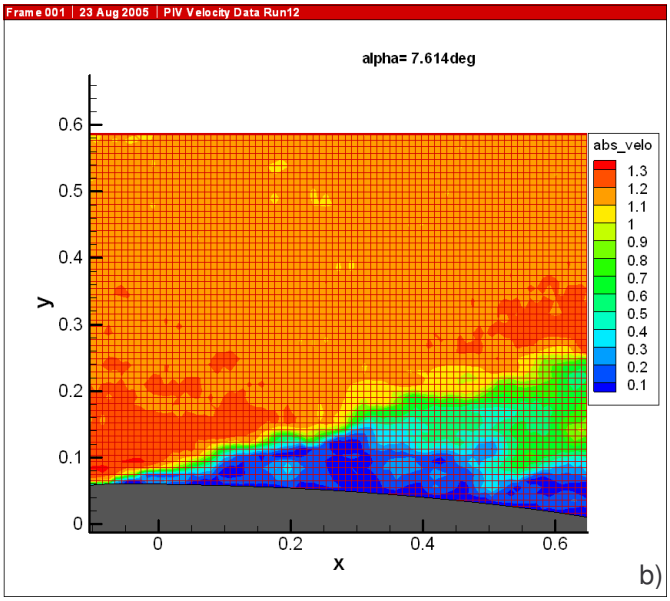

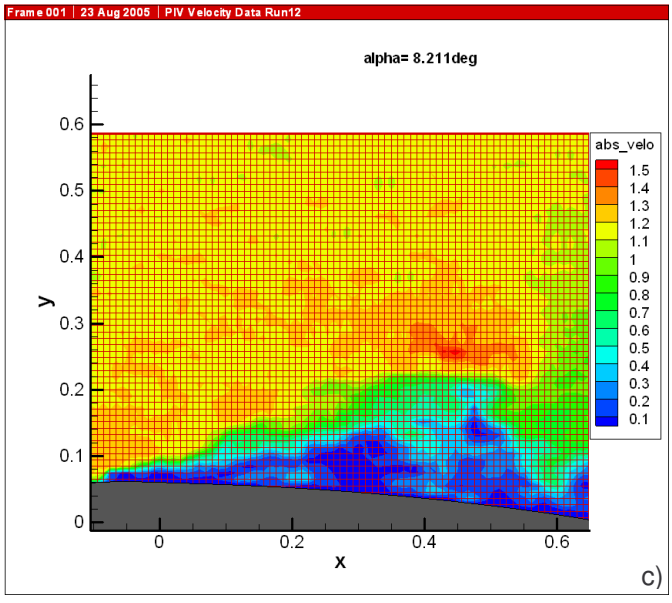

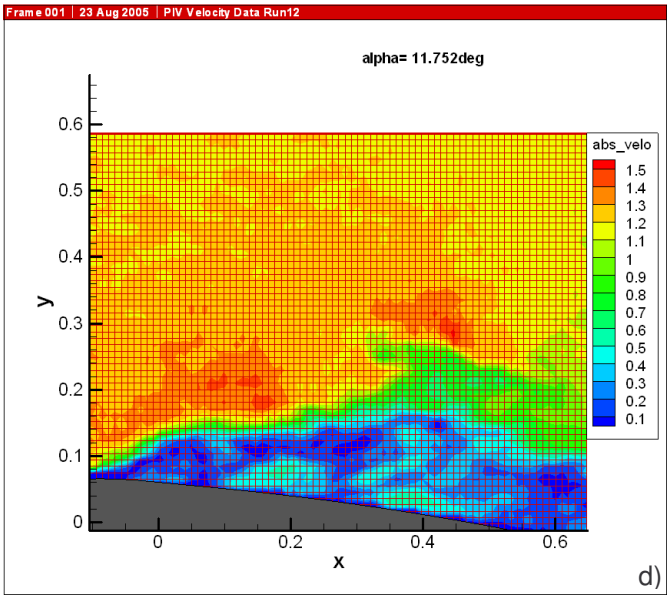

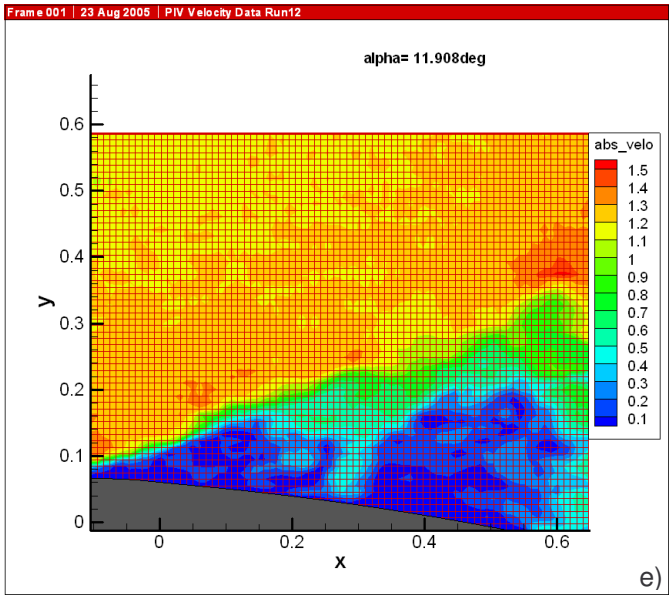

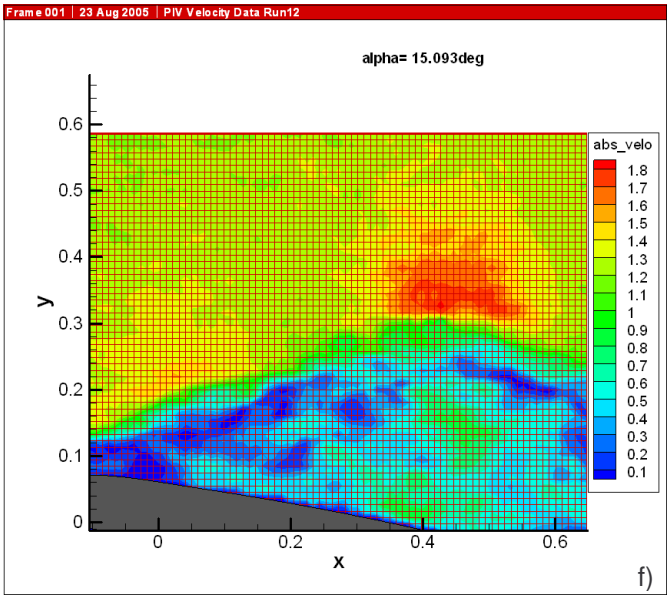

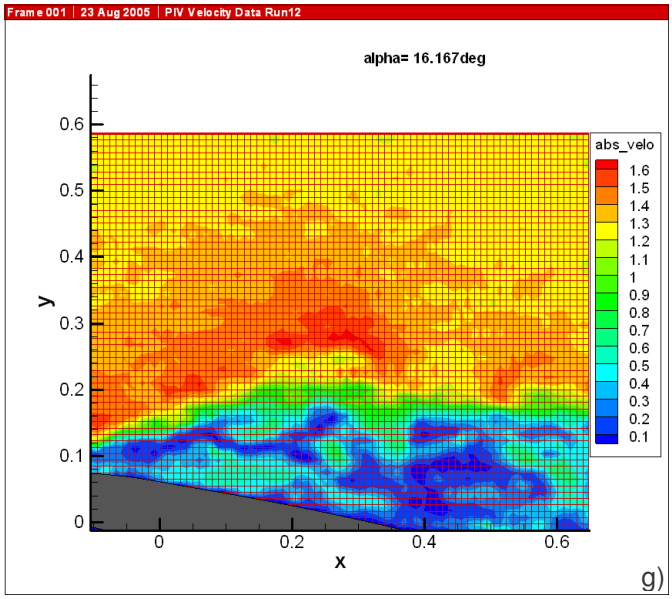

Fig. 18: Absolute velocity U/U_∞ evolution during down stroke motion for α (t) =11deg+-6deg.

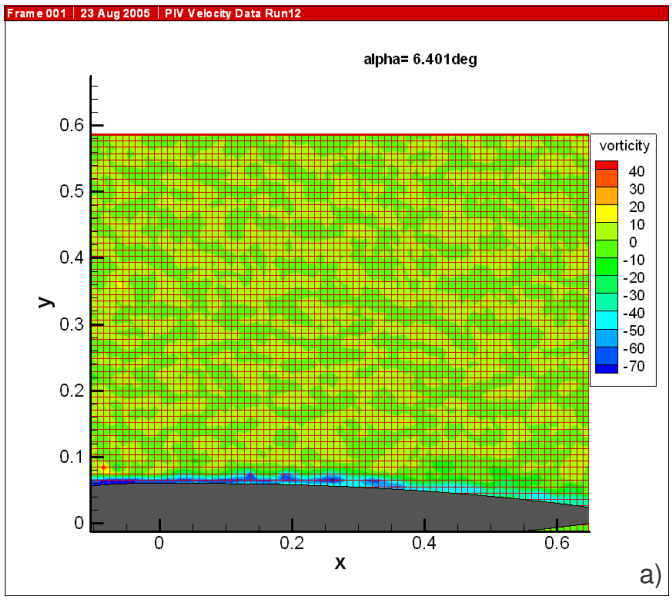

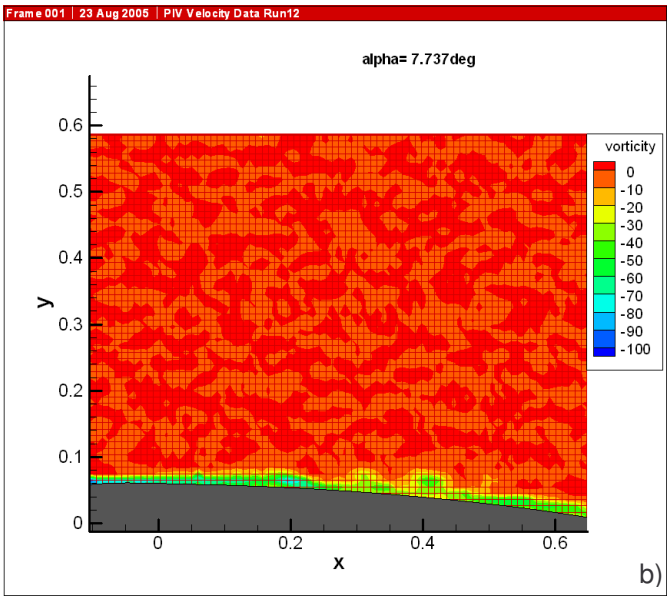

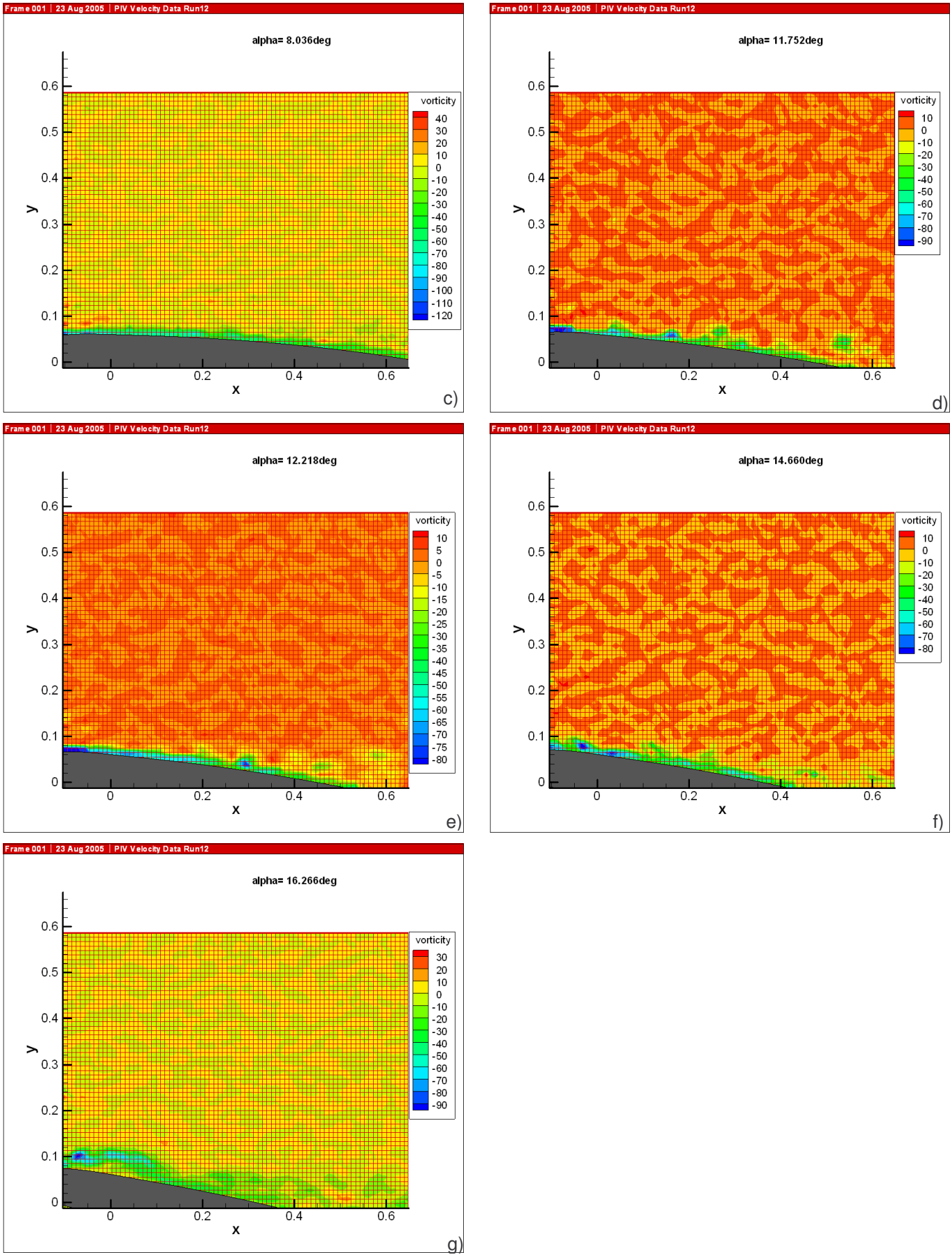

Fig. 19: Ω local vorticity evolution during up stroke motion for α (t) =11deg+-6deg.

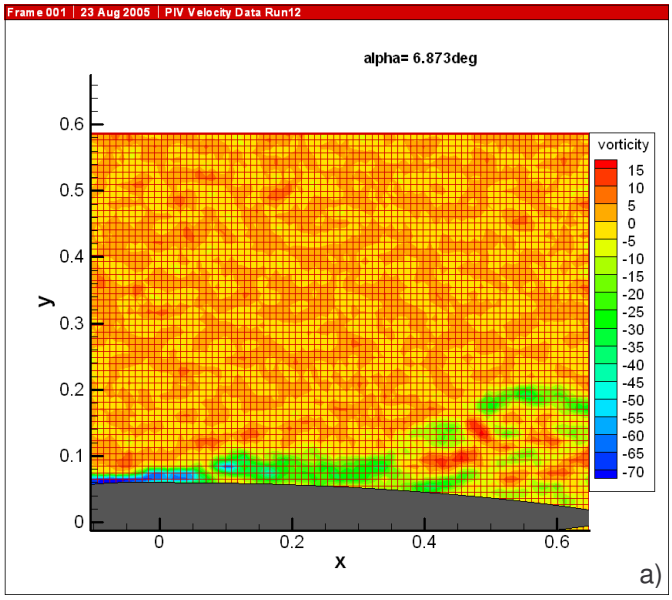
Frame 001 | 23 Aug 2005 | PIV Velocity Data Run12
alpha= 6.873deg
vorticity
15
10
5
0
-5
-10
-15
-20
-25
-30
-35
-40
-45
-50
-55
-60
-65
-70
y
x
0
0.1
0.2
0.3
0.4
0.5
0.6
a)

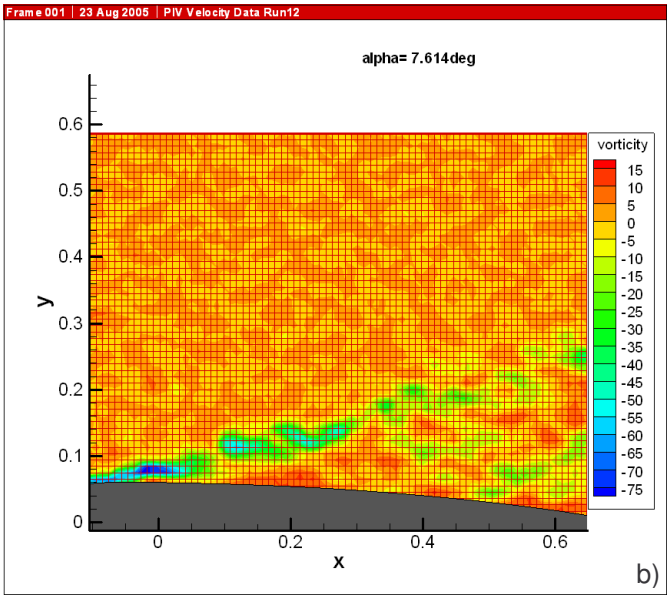
Frame 001 | 23 Aug 2005 | PIV Velocity Data Run12
alpha= 7.614deg
vorticity
15
10
5
0
-5
-10
-15
-20
-25
-30
-35
-40
-45
-50
-55
-60
-65
-70
-75
y
x
0
0.1
0.2
0.3
0.4
0.5
0.6
b)

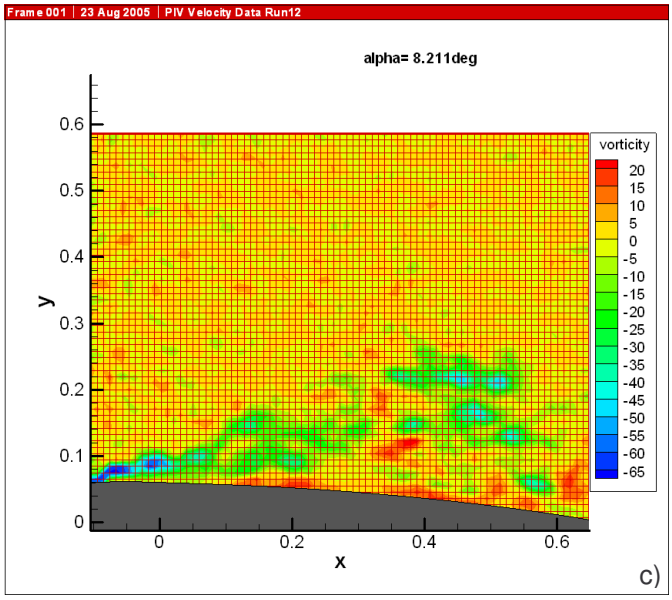
Frame 001 | 23 Aug 2005 | PIV Velocity Data Run12
alpha= 8.211deg
vorticity
20
15
10
5
0
-5
-10
-15
-20
-25
-30
-35
-40
-45
-50
-55
-60
-65
y
x
0
0.1
0.2
0.3
0.4
0.5
0.6
c)

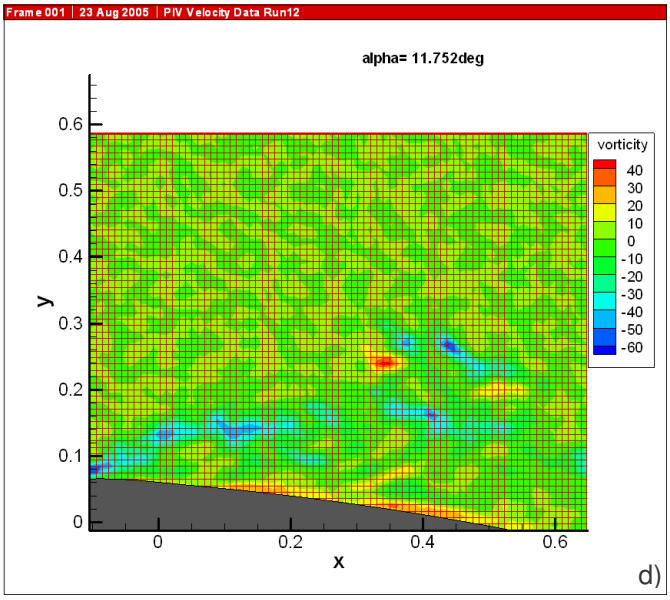
Frame 001 | 23 Aug 2005 | PIV Velocity Data Run12
alpha= 11.752deg
vorticity
40
30
20
10
0
-10
-20
-30
-40
-50
-60
y
x
0
0.1
0.2
0.3
0.4
0.5
0.6
d)

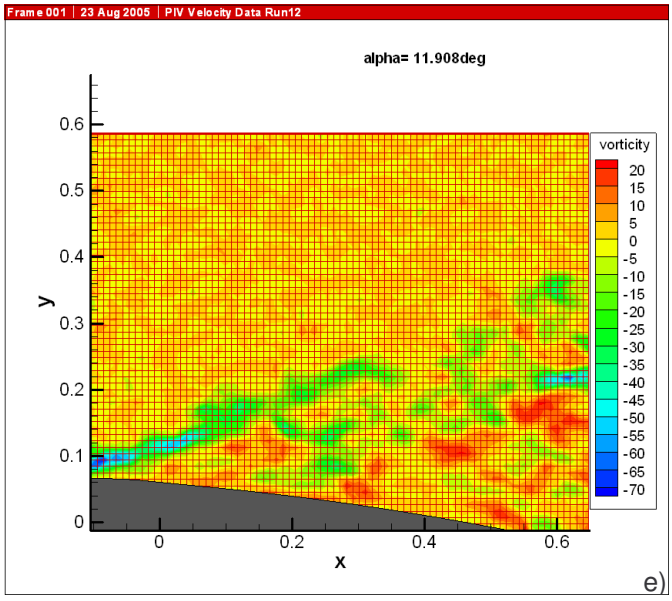
Frame 001 | 23 Aug 2005 | PIV Velocity Data Run12
alpha= 11.908deg
vorticity
20
15
10
5
0
-5
-10
-15
-20
-25
-30
-35
-40
-45
-50
-55
-60
-65
-70
y
x
0
0.1
0.2
0.3
0.4
0.5
0.6
e)

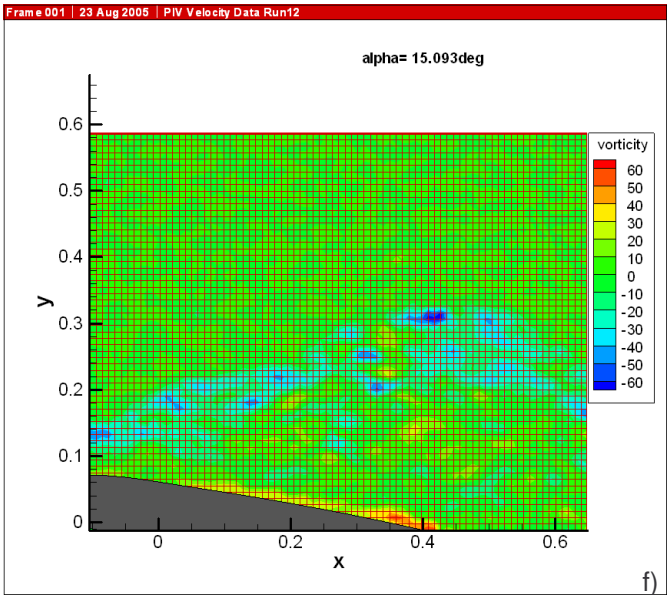
Frame 001 | 23 Aug 2005 | PIV Velocity Data Run12
alpha= 15.093deg
vorticity
60
50
40
30
20
10
0
-10
-20
-30
-40
-50
-60
y
x
0
0.1
0.2
0.3
0.4
0.5
0.6
f)

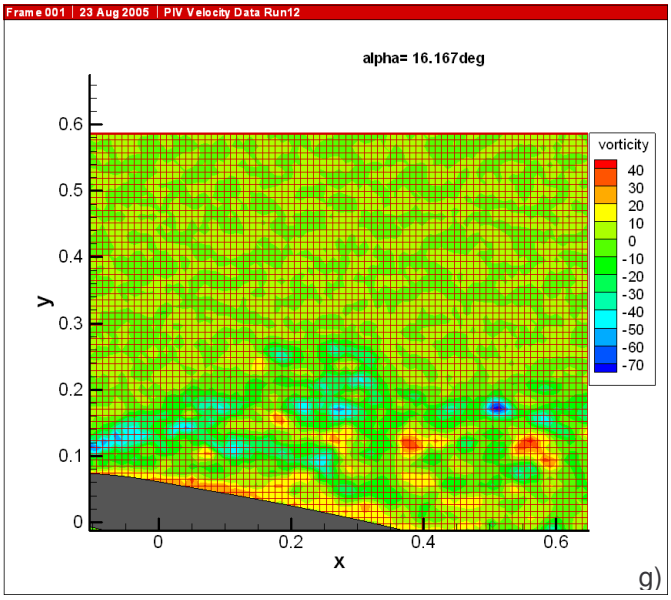

Fig. 20: Ω local vorticity evolution during down stroke motion for α (t) =11deg+-6deg.